Patent Office

23 FEBRUARY 2000

INVESTOR IN PEOPLE

09/914081

GB 00/692

PRIORITY DOCUMENT

SUBMITTED OR TRANSMITTED IN COMPLIANCE WITH RULE 17.1(a) OR (b)

The Patent Office
Concept House
Cardiff Road
Newport
South Wales
NP10 8QQ

RECD 22 MAR 2000

WIPO PCT

4

I, the undersigned, being an officer duly authorised in accordance with Section 74(1) and (4) of the Deregulation & Contracting Out Act 1994, to sign and issue certificates on behalf of the Comptroller-General, hereby certify that annexed hereto is a true copy of the documents as originally filed in connection with the patent application identified therein.

In accordance with the Patents (Companies Re-registration) Rules 1982, if a company named in this certificate and any accompanying documents has re-registered under the Companies Act 1980 with the same name as that with which it was registered immediately before re-registration save for the substitution as, or inclusion as, the last part of the name of the words "public limited company" or their equivalents in Welsh, references to the name of the company in this certificate and any accompanying documents shall be treated as references to the name with which it is so re-registered.

In accordance with the rules, the words "public limited company" may be replaced by p.l.c., plc, P.L.C. or PLC.

Re-registration under the Companies Act does not constitute a new legal entity but merely subjects the company to certain additional company law rules.

Signed M Cook

Dated 2-3-00

ficial use

PATENT OFFICE A 23 FEB 1999 LONDON

24FEB99 E427787-1 003312
P01/7700 0.00 - 9904166.7

Your reference 230P80316

Notes
Please type, or write in dark ink using CAPITAL letters. A prescribed fee is payable for a request for grant of a patent. For details, please contact the Patent Office (telephone 071-438 4700).

Rule 16 of the Patents Rules 1990 the main rule governing the completion and filing of this form.

The Patent Office

Request for grant of a Patent

Form 1/77

Patents Act 1977

❶ Title of invention

1 Please give the title of the invention: Radiation Imaging

9904166.7

❷ Applicant's details

❷ Do not give trading styles, for example, 'Trading as XYZ company', nationality or former names, for example, 'formerly (known as) ABC Ltd' as these are not required.

❑ **First or only applicant**

2a If you are applying as a corporate body please give:

Corporate name: Toshiba Research Europe Limited

Country *(and State of incorporation, if appropriate)*: United Kingdom.

Warning
After an application for a Patent has been filed, the Comptroller of the Patent Office will consider whether publication or communication of the invention should be prohibited or restricted under Section 22 of the Patents Act 1977 and will inform the applicant if such prohibition or restriction is necessary. Applicants resident in the United Kingdom are also reminded that under Section 23, applications may not be filed abroad without written permission unless an application has been filed not less than 6 weeks previously in the United Kingdom for a patent for the same invention and either no direction prohibiting publication or communication has been given, or any such direction revoked.

2b If you are applying as an individual or one of a partnership please give in full:

Surname

Forenames

2c **In all cases**, please give the following details:

Address: Cambridge Research Laboratory,
260 Cambridge Science Park, Milton Road,
Cambridge, CB4 4WE, England.
United Kingdom.

UK postcode *(if applicable)*

Country

ADP number *(if known)*: 7514136001

.d, 2e and 2f: *If there are further applicants please provide details on a separate sheet of paper.*

❑ **Second applicant *(if any)***

2d If you are applying as a corporate body please give:

Corporate name

Country *(and State of incorporation, if appropriate)*

2e If you are applying as an individual or one of a partnership please give in full:

Surname

Forenames

2f **In all cases**, please give the following details:

Address

UK postcode *(if applicable)*

Country

ADP number *(if known)*

❸ *An address for service in the United Kingdom must be supplied*

Please mark correct box

❸ Address for service details

3a Have you appointed an agent to deal with your application?

Yes ☒ No ☐ ➡ ***go to 3b***

⬇ ***please give details below***

Agent's name Marks & Clerk

Agent's address 57-60 Lincoln's Inn Fields
LONDON
WC2A 3LS.

Postcode

Agent's ADP number 18001

3b: *If you have appointed an agent, all correspondence concerning your application will be sent to the agent's United Kingdom address.*

3b If you have not appointed an agent please give a name and address in the United Kingdom to which all correspondence will be sent:

Name

Address

Postcode

Daytime telephone number *(if available)*

ADP number *(if known)*

Reference number

4 Agent's or applicant's reference number *(if applicable)* 230P80316

❺ Claiming an earlier application date

5 Are you claiming that this application be treated as having been filed on the date of filing of an earlier application?

Please mark correct box

Yes ☐ **please give details below** No ☒ **go to 6**

❑ number of earlier application or patent number

❑ filing date *(day month year)*

❑ and the Section of the Patents Act 1977 under which you are claiming:

Please mark correct box

15(4) (Divisional) ☐ 8(3) ☐ 12(6) ☐ 37(4) ☐

❻ Declaration of priority

❻ If you are declaring priority from a PCT Application please enter 'PCT' as the country and enter the country code (for example, GB) as part of the application number.

Please give the date in all number format, for example, 31/05/90 for 31 May 1990.

6 If you are declaring priority from previous application(s), please give:

Country of filing	Priority application number *(if known)*	Filing date *(day, month, year)*

The answer must be 'No' if:
- any applicant is not an inventor
- there is an inventor who is not an applicant, **or**
- any applicant is a corporate body.

7 Inventorship

7 Are you (the applicant or applicants) the sole inventor or the joint inventors?

Please mark correct box

Yes ☐ No ☒ ➡ ***A Statement of Inventorship on Patents Form 7/77 will need to be filed (see Rule 15).***

Please supply duplicates of claim(s), abstract, description and drawing(s).

8 Checklist

8a Please fill in the number of sheets for each of the following types of document contained in this application.

Continuation sheets for this Patents Form 1/77 — 8

Claim(s) 8 Description 33

Abstract 1 Drawing(s) 19 + 9 (formal)

8b Which of the following documents also accompanies the application?

Please mark correct box(es)

Priority documents *(please state how many)* —

Translation(s) of Priority documents *(please state how many)* —

Patents Form 7/77 – Statement of Inventorship and Right to Grant *(please state how many)* 1 ✓

Patents Form 9/77 – Preliminary Examination/Search 1 ✓

Patents Form 10/77 – Request for Substantive Examination 1 ✓

You or your appointed agent (see Rule 90 of the Patents Rules 1990) must sign this request.

9 Request

I/We request the grant of a patent on the basis of this application.

Please sign here ➡ Signed Marks & Clerk Date 23 - 2 - 99 *(day month year)*

A completed fee sheet should preferably accompany the fee.

Please return the completed form, attachments and duplicates where requested, together with the prescribed fee to:

❑ ***The Comptroller***
The Patent Office
Cardiff Road
Newport
Gwent
NP9 1RH

or

❑ ***The Comptroller***
The Patent Office
25 Southampton Buildings
London
WC2A 1AY

Radiation Imaging

The present invention relates to the field of imaging samples with radiation in the infra-red (IR) frequency range. More specifically, the present invention relates to apparatus and methods for improving contrast in images obtained using electromagnetic radiation in the higher Gigahertz (GHz) and the Terahertz (THz) frequency ranges. However, in such imaging technology, all such radiation is colloquially referred to as THz radiation, especially that in the range from 200GHz to 84Thz.

Recently, there has been much interest in using THz radiation to look at a wide variety of samples using a range of methods. THz radiation has been used for both imaging samples and obtaining spectra. Recently, work by Mittleman *et al*, IEEE Journal of Selected Topics in Quantum Electronics, Vol. 2, No. 3, September 1996, page 679 to 692 illustrates the use of using THz radiation to image various objects such as a flame, a leaf, a moulded piece of plastic and semiconductors.

THz radiation penetrates most dry, non metallic and non polar objects like plastics, paper, cardboard and non polar organic substances. Therefore, THz radiation can be used instead of x-rays to look inside boxes, cases etc. THz has lower energy, non-ionising photons than X-rays, hence, the health risks of using THz radiation are expected to be vastly reduced compared to those using conventional X-rays.

The use of THz imaging for medical purposes has also been suggested in the above referenced paper. However, it has previously been believed that strong-water absorption prevents the use of THz in many bio-medical research areas. Previously, a large amount of THz imaging has been analysed on the basis of obtaining contrasts between strongly water absorbing regions and non strongly water absorbing regions.

The present invention addresses the above problems and is concerned with methods for enhancing image contrasts in such THz images to allow THz to be used to not only image contrast based on water absorption but to allow a fine contrast to be shown in THz imaging over a range of different samples.

In a first aspect, the present invention provides a method of imaging a sample, the method comprising the steps of:

a) irradiating the sample to be imaged with pulsed electro-magnetic radiation with a plurality of frequencies in the range from 50 GHz to 84 THz;

b) subdividing an area of the sample into a two dimensional array of pixels, and detecting radiation from each pixel over a plurality of frequencies;

c) generating an image from the radiation detected in step (b) using a frequency or a selection of frequencies from the plurality of frequencies in the incident pulsed electro-magnetic radiation.

Preferably, the sample is irradiated with pulsed electro-magnetic radiation with a plurality of frequencies in the range from 100 GHz to 20 THz; more preferably from 500 GHz to 10 THz.

The detected radiation may be analysed for a single frequency, or, it may be analysed over a selected frequency range. A selected frequency range is taken to be a frequency range which is typically, less than a third of the total frequency range of the pulsed e-m radiation used to irradiate the sample. More preferably, the selected frequency range is less than 10% of the total frequency range of the pulsed e-m radiation used to irradiate the sample.

For example, it has previously been mentioned that water is a strong absorber of THz. There are 'windows' in the water absorption spectra from 50 GHz to 500 GHz, from 30 THz to 45 THz and from 57 THz to 84 THz. If the sample is a irradiated with a range of frequencies from 50 Ghz to 84 THz, it may be preferable to generate the image using one or more of the following selected frequency ranges: 50 GHz to 500 GHz, 30 THz to 45 THz and 57 THz to 84 THz. The image may be generated by integrating over the selected frequency range.

Thus, the present invention allows an image to be created from single frequency or from a selected frequency range. Also, the present invention allows a plurality of images to be derived from a plurality of frequencies or allows a single image to be derived from data from two or more distinct frequencies.

The present invention can either be used to image a sample by detecting radiation transmitted through the sample or reflected from the sample.

The image or images generated by the present invention my be displayed in a number of ways. For example, the method of the first aspect of the present invention may further comprise the step of displaying a sequence of images generated in step (c) for a plurality of different frequencies.

The image generated in step (c) may be scanable through a continuum of frequencies. Alternatively, the image generated in step (c) can be stepped through a plurality of discrete frequencies.

For many imaging contrast techniques discussed herein, a reference signal is required. Ideally, the reference signal is obtained from THz radiation which has not been passed through or reflected from the area of the sample which is to be imaged.

The reference signal may be obtained from a fraction of the electro-magnetic pulsed radiation which has not been passed through the sample, alternatively, the

reference signal may be obtained by passing the pulsed electro-magnetic radiation through a different part of the sample. For example, the present invention may be used to image tumours tissue, the area of the sample which is to be imaged would the tumour, the reference signal could be obtained by passing the radiation through a healthy part of the tissue. The reference signal may also be measured when the sample is absent. For example, the reference signal could be measured before the sample is positioned in the path of the radiation beam or the reference signal could be measured after the sample has been imaged.

In general, the present invention will be performed using imaging apparatus which is configured to detect temporal data at each pixel. Preferably, the data is Fourier transformed to give the complex THz electric field in the frequency domain $E(\omega)$.

The image can be obtained in a number of ways from the complex THz electric field $E(\omega)$, e.g.:

(i) The power spectrum $P_{sample}(\omega)$ of the sample and the power spectrum $P_{ref}(\omega)$ of the reference signal may be calculated. The image could then be generated by plotting the difference between the two Power spectrums for a given frequency for each pixel at a selected frequency over integrated over a selected frequency range.

(ii) The power spectrum P_{sample} of the sample and the reference power spectrum P_{ref} may be divided to give the transmittance. The transmittance may then be plotted for each pixel at a selected frequency over integrated over a selected frequency range.

(iii) The frequency dependent absorption coefficient $\alpha(\omega)$ may be calculated from the complex electric field $E(\omega)$ and plotted for each pixel at a selected frequency over integrated over a selected frequency range.

(iv) The frequency dependent refractive index $\eta(\omega)$ may also be calculated from the complex electric field and plotted for each pixel at a selected frequency over integrated over a selected frequency range.

The detected temporal electric field contains both phase and amplitude information which give a complete description of the complex dielectric constant of the medium in the beam path. The sample to be characterised is inserted into the beam and the shape of the pulses that have propagated through the sample or have been reflected from the sample are compared with the reference temporal profile acquired without the sample. The ratio of the complex electric field $E(\omega)$ and the reference signal $E_{ref}(\omega)$ is calculated to give the complex response function of the sample, $S(\omega)$. In the most simple case, the complex response function is given by:

$$S(\omega) = \frac{E(\omega)}{E_{ref}(\omega)} \propto \exp\left(\frac{i\omega d}{c}(\eta(\omega)-1)\right)\exp(-\alpha(\omega)d) \qquad (1)$$

where d is the sample thickness, c is the velocity of light in vacuum, η is the refractive index and α is the absorption coefficient. The experimental absorption coefficient $\alpha(\omega)$ and the refractive index $\eta(\omega)$ may then be easily extracted from the magnitude $M(\omega)$ and the phase $\phi(\omega)$ of $S(\omega)$, respectively, according to

$$\alpha(\omega) = -\tfrac{1}{d}\ln(M(\omega)) \qquad (2)$$

$$\eta(\omega) = 1 + \left(\tfrac{c}{\omega d}\right)\phi(\omega) \qquad (3)$$

Additional terms may be included in equations (1) to (3) to account for reflections at dielectric interfaces of a sample, thus allowing accurate analysis of multilayered samples.

These parameters are simply related to the complex dielectric function $\varepsilon(\omega)$ of the sample

$$\varepsilon(\omega) = (\eta(\omega) + ik(\omega))^2 = (\eta(\omega) + i\alpha(\omega)c / 2\omega)^2 \tag{4}$$

The data derived as discussed in (i) to (iv) above, may be directly plotted either as a colour or a grey scale image where the colour or shade of grey of each pixel represents a given magnitude.

Instead of a single frequency, a selected frequency range could be chosen and the result and data of (i) to (iv) integrated over that range. The integrated data could then be plotted.

It may also be preferred to subdivide the magnitude of the data process in accordance with any of (i) to (iv) above into various bands. For example, all data below a certain value could be assigned the value 0, all data in the next magnitude range could be assigned the value 1, etc. These ranges may have equal widths in magnitude or they may have different widths. Different widths may be preferable to enhance contrast e.g. to emphasise contrast in regions of the sample where there is little variation in the sample absorption of THz.

Preferably, the present invention uses two or more frequencies. The data from say two frequencies is processed in accordance with any of (i) to (iv) above. The data is then banded as described for a single frequency above.

The data may be split into two hands, one assigned the value "0" and the other "1". The data from both frequencies can then be added together using a rule such as a Boolean algebraic expression e.g. AND, OR, NOT, NAND, XOR, etc.

Of course, the present invention also allows images to be compared from two different frequencies. This may be particularly useful to identify a substance where the absorption to THz changes over a certain frequency range.

Other methods are also possible for such THz imaging. It is known to plot the maximum or minimum of the electric field. Indeed, this has been done by Mittleman in the earlier reference paper. However, far greater contrast is achieved by plotting the peak to peak signal, i.e. the distance between the minimum and maxima of the electric field. Therefore, in a second aspect, the present invention provides a method for imaging a sample, the method comprising the steps of :

a) irradiating the sample to be imaged with a pulsed electro-magnetic radiation with a plurality of frequencies in the range from 50 GHz to 84 THz;

b) subdividing an area of the sample into a two dimensional array of pixels, and detecting radiation from each pixel over a plurality of frequencies;

c) generating an image from the radiation detected in step (b) by calculating the difference between the magnitude of a maxima and a minima of the radiation detected in step (b) for each pixel.

Preferably, the main peak minima and maxima are chosen i.e. the highest and lowest parts of the temporal trace.

More preferably, the sample is irradiated with pulsed electro-magnetic radiation with a plurality of frequencies in the range from 100 GHz to 20 THz;

It is also known to derive temporal information from the data. For example, the time difference between the maxima of the electric field which is passed through the sample and the field which is not passed through or reflected from the area of the sample, which is to imaged, can be plotted. However, there has been no suggestion of plotting the temporal difference between the maximum and the minimum of the electric field. This provides data on the frequency dependent absorption. Therefore, in a third

7

aspect, the present invention provides a method for imaging a sample, the method comprising the steps of :

a) irradiating the sample to be imaged with pulsed electro-magnetic radiation with a plurality of frequencies in the range from 50 GHz to 84 THz;

b) subdividing an area of the sample into a two dimensional array of pixels, and detecting radiation from each pixel over a plurality of frequencies;

c) generating an image from the radiation detected in step (b) by calculating the difference between the temporal positions of a maxima and a minima of the radiation detected in step (b) for each pixel.

Further aspects of the present invention provide apparatus for effecting the methods, respectively, of the first, second and third aspects of the present invention, each respectively comprising means for carrying-out each of the steps of those methods.

Preferably, the main peak minima and maxima are chosen i.e. the highest and lowest parts of the temporal trace.

More preferably, the sample is irradiated with pulsed electro-magnetic radiation with a plurality of frequencies in the range from 100 GHz to 20 THz;

To obtain even better contrast, the temporal difference between the maximum and the minimum field may also multiplied by a value of the field at that pixel. For example, the minimum, maxima or difference between the minima and maxima.

As mentioned above, the method of the present invention is suitable for medical imaging and is ideally suited to probing certain tissue abnormalities and conditions. It is also useful for imaging items inside containers, for investigating the internal structure

and composition of foods, as well as authentication of documents, labels, banknotes or other printed matter and for analogous security applications. Some particular medical applications will now be explained in more detail.

Cancerous tissue:

Normal tissue contains a large number of mature cells of uniform shape and size. Each cell is characterised by a nucleus of uniform size.

Benign neoplasm:

Benign neoplasm involve cellular proliferation of adult or mature cells growing slowly in an orderly manner in a capsule. These tumours do not invade surrounding tissue but may cause harm through pressure on vital structures within an enclosed structure such as the skull.

Malignant cells:

A malignant cell is one in which the basic structure and activity have become deranged in a manner that is unknown and from a cause or causes that are still poorly understood. The malignant cells lose the normal specialised function of the normal cell or may take on new characteristics and functions. A characteristic of malignant cells that can be observed through a microscope is loss of differentiation, or loss of likeness to the original cell (parent tissue) from which the tumour growth originated. This loss of differentiation is called anaplasia, and its extent is a determining factor in the extent of malignancy of the tumour. Anaplasia is one of the most reliable indicators of malignancy. It is seen only in cancers and does not appear in benign neoplasms.

Other characteristics of malignant cells that can be seen through a microscope are the presence of nuclei of various sizes, many of which contain unusually large

amounts of chromatin, and the presence of mitotic figures (cells in the provision of division), which denotes rapid and disorderly division of cells. The proportion of cells actively proliferating in malignant tumours is generally greater than that of normal cells. Malignant cells have no enclosing capsule; thus they invade adjacent or surrounding tissue.

Spread of Cancer:

It has been calculated in general that a tumour mass will double in size 30 times before it is 1cm in size, when there is a chance for clinical detection by conventional means. The rate of growth of a malignant neoplasm determines its capacity to spread. Cancer may spread by direct extension, by gravitational metastasis, or by metastatic spread.

Direct extension or invasion of neighbouring tissue produces the typical local effects of ulcerating, bulky, hemorhagic masses or indurative, fibrosing lesions with tissue fixation, distortion of structure, and pitting of the skill seen in some breast cancer. Infection may accompany this spread.

Gravitional metastasis involves erosion of cancer cells in the body cavities and their dropping onto the serous membrane lining in the cavity.

Metastatic spread occurs when the cancer cells invade vascular or lymphatic channels and travel to distant parts of the body where implantation occurs. In metastatic spread, there is almost always a high degree of histologic, cytologic, and functional similarity between the primary cancer and these metastases. Consequently, the type of cell and probable site of the primary tumour can be identified from the morphology of the metastasies. In addition, the mestastes usually mimic the primary tumour in the formation of cell products and secretions.

Anaplasia should result in the modification of the transmission, absorption, and reflection properties of tissue 50GHz-40THz frequency range which can be studied by the method of the present invention. The loss of differentiation and additional ulcerating, bulky, hemorhagic masses or indurative, fibrosing lesions with tissue fixation, distortion of structure should modify the following quantities which can be imaged by a method of the present invention.

Refractive index change:

For a given thickness, the probability of interaction between radiation and tissue is dependent on the density of the material. The appearance of fibrous material and additional (mutated) cells in a tumorous region suggests that the density of the tissue in this region will be modified relative to that of healthy tissue, leading to a density change. This in turn should modify the refractive index of the medium (either at a fixed frequency ω or over a range of frequencies) relative to that in normal tissue. These changes in the refractive index can be detected by either 1) simply, by shifts in the time domain of a transmitted or reflected THz pulse or 2) least squares fits to frequency domain information, which will yield the refractive index at each frequency $\eta(\omega)$. In the cancerous regions, we expect increases in the refractive index due to increases in the density of cells in that region. However, exclusion of water in the cancer will also modify the refractive index. Due to either effect, we would anticipate using refractive index determination at different pixels in the image, using either 1), 2) or a combination of the two, as an important contrast mechanism.

Thickness change: Changes in thickness d between abnormal and normal tissue will lead to changes in either

a) the absorption in a given region $a(\omega)d$ or

b) the time delay of the pulse in that region $\eta(\omega)d$.

Both a) and b) can be determined using electric field and time domain spectra, respectively, forming the basis of a contrast mechanism. Because malignant cancer

grows rapidly relative to the tissue which it invades, it is likely that a malignant tumour and the normal tissue adjacent to it will differ appreciably in thickness, which can be determined by the methods of the present invention using a) and/or b) above.

Absorption coefficient change: For a given thickness, the probability of interaction between radiation and tissue is dependent on the density of the material. The appearance of fiborous material and additional (mutated) cells in a tumourous region suggests that the density of the tissue in this region will be modified relative to that of healthy tissue, leading to a density change between normal and cancerous tissue. The linear attenuation coefficient $a(\omega)$ (usually quoted in units of cm^{-1}) is dependent on the density of the material. Thus, if a tumour represents a larger amount of tissue in the same volume, the linear attenuation coefficient $a(\omega)$ will increases proportionally to the increase in density. For a given thickness, this change will manifest itself as increased absorption in the tumour relative to the normal tissue.

Convolved with such density-induced changes in $a(\omega)$ will be variations in $\alpha(\omega)$ due to changes in the composition of the tissue itself. Changes in chemical composition are the most obvious reason for this. For example, the presence of ulcerating, bulky, hemorhagic masses in tumours implies a change in chemical composition relative to healthy tissue. In certain types of malignant tumours such as cytologic anaplasia, there is increased or altered nucleic acid synthesis in growing tissue, which implies a change in chemical content. Moreover, simpler changes such as the exclusion or inclusion of additional water in a tumour will change its chemical composition relative to that of healthy tissue.

$\alpha(\omega)$ may also change in the THz range due to increased disorder in the system. Thus, even if there is no change in the type of molecules in tumourous vs normal tissue, the tumour is likely to be more disordered in terms of the arrangements between cells. A similar phenomenon occurs in liquids, where increasing disorder (or lack of crystallisation) leads to increased absorption. It is therefore probable that $\alpha(\omega)$ will be larger in randomly arranged tumour tissue than in more "regularly arranged" tissues.

The present invention will now be described by way of example and with reference to the following non-limiting embodiments in which:

Figure 1 shows a typical THz time domain data obtained from imaging a sample;

Figure 2 shows a power spectrum of a THz trace originally measured in the time domain;

Figure 3a is an image of a pork sample at visible light wavelengths and figure 3b is the same pork sample at THz frequencies;

Figure 4 shows three power spectra for different pixels of the image of figure 3b;

Figure 5 shows data for absorption coefficient for dried pork skin and dried pork kidney samples;

Figure 6 shows THz electric field data and time domain and power spectrum frequency domain for different types of chicken tissue;

Figure 7 shows power spectra obtained from the data of Figure 6 plotted on a single axis;

Figure 8 shows a visible image of a spider mounted over a hole in the metal plate;

Figure 9 shows a visible image of the spider in a box with the box open (Figure 9a) and the box closed (Figure 9b);

Figure 10 shows the THz image of the spider in the box of Figure 9b;

Figure 11 shows the THz electric field and power spectrum derived from a blood sample;

Figure 12 shows the THz electric field and power spectra derived from a water sample;

Figure 13a shows a visible image of a commercial package transistor, Figure 13b shows a THz image of Figure 13a and Figure 13c shows a cut away image of the transistor of Figure 13a;

Figure 14a shows the THz image of doped and undoped GaAs, Figure 14b shows the same sample using visible radiation;

Figure 15 shows a monochromatic image of the semiconductor of Figures 14 and 15;

Figure 16 shows a monochromatic image similar to Figure 15 but at a different frequency;

Figure 17 is a schematic diagram of a THz imaging system;

Figure 18 shows a variation of imaging system of figure 17;

Figure 19 shows a schematic of a detection section which can be used with the imaging system of Figure 18;

Figure 20 shows the imaging system of Figure 18 with the detection section of Figure 19;

Figure 21 shows a variation on the imaging section of Figure 20;

Figure 22 shows a variation on the imaging section of Figure 20;

Figure 23 shows a variation on the imaging section of Figure 20;

Figure 24 shows a further example of an imaging; and

Figure 25 shows another example of an imaging system.

The sample is imaged by irradiating with pulsed electro-magnetic radiation in 100GHz to 20THz. The THz radiation is either passed through the sample or reflected from the sample. Figure 1 shows a typical trace of detected electric field over time detected from the sample for a single pixel. If there is a variation in the sample composition from pixel to pixel, then this will show up in the THz trace for each pixel.

As can be seen from Figure 1, there is a vast amount of information obtained for each pixel therefore, the information needs to be processed to provide a meaningful image. There are four main parameters which can be derived from this time dependent signal. These are: the maxima of the electric field (E_1), the minima of the electric field (E_2), the temporal position of the maxima of the electric field (T_1) and the temporal position of the minima of the electric field (T_2).

To obtain a THz image, one or more of these parameters may be plotted directly. However, further contrast may be obtained by plotting the following functions:

1. The peak to peak height i.e. E_1 and E_2;

2. The difference in the temporal spacing between a position of the maxima E_1 and the position of the minima E_2 i.e. T_1-T_2. This parameter is particularly useful as it gives information on the frequency dependent absorption of the sample.

3. The product of the temporal peak position with one or more electric field parameters. For example:

$$(T_2-T_1) \times E_1$$

$$(T_2-T_1) \times E_2$$

$$T_2-T_1 \times (E_1+E_2)$$

Further information may also be obtained from Figure 1 by performing a frequency analysis. Figure 2 shows a power spectrum for a typical trace. The power spectrum is obtained in the conventional way from Fourier transforming the temporal data (i.e. the type of data shown in Figure 1). The magnitude of the signal is plotted logarithmically on the y-axis and the frequency is plotted on the x-axis. The data for Figure 2 was derived from a sample which had regions of fat, kidney and meat. This will be described later in more detail with reference to Figure 3. A reference signal is also shown which is the power spectrum of radiation which has not passed through the sample. By viewing the data in this form, the spacing between the data (along the y axis) for the three tissue types is seen to vary with frequency. Therefore, by choosing an appropriate frequency (f_{select}) an image with strong contrast may be obtained.

Also, to distinguish certain tissue types it is often advantageous to plot the image at two separate frequencies for comparison. This is particularly useful when there is little contrast between the tissue types at various frequencies. For example, taking the data of Figure 2, it is seen that the power spectrum corresponding to kidney tissue and fat tissue has an almost identical value at 1THz. Therefore, in an image generated at this frequency, both fat and kidney would look very similar. However, looking at the trace at around 2.5THz, it is seen that the kidney data has a similar value

to that of the meat data. Therefore, at an image taken at 2.5THz there is very little contrast between the meat and the kidney data. However, comparing the image taken at 1THz with the image taken at 2.5THz, allows the three tissue types to be equally distinguished. Two or more images at different frequencies can also be compared by a mathematical operation. For example, the data taken at 2.5THz could be subtracted from the data taken at 1THz to clearly show the characteristic signal due to absorption by kidney tissue. Other mathematical operations are also possible such as multiplication, addition, and division etc.

To further enhance contrast, the data can be subdivided into a series of bands based on magnitude. In Figure 2, four bands are shown. Each of these bands can be assigned a single numerical value and this data can then be plotted. In the data of Figure 2, it can be seen by assigning a single value to band 2 and a single integer value to band 2 and a single integer value to band 3 where substantially enhanced contrasts between the fat tissue and the kidney tissue. This analysis can further be extended to just two amplitude bands. In one amplitude band, the amplitude is assigned a value of zero and in the second amplitude band the amplitude is assigned a value of one. This analysis allows data at two different frequencies, f_1 and f_2 to be compared using certain rules. Such a rule could be:

Signal (f_1)	**Signal (f_2)**	**New Value**
0	0	1
1	0	2
0	1	3
1	1	4

Also, certain Boolean algebraic expressions could be used, for example, AND, NAND, XOR, OR, NOR. For an AND comparison, the following table would be used:

Signal (f_1)	**Signal (f_2)**	**New Value**
0	0	0
1	0	0
0	1	0
1	1	1

Instead of the power spectrum, the frequency dependent absorption coefficient $a(\omega)$ or the frequency dependent refractive index $\eta(\omega)$ could be analysed in the same way as the power spectrum.

Figures 3a and 3b show images obtained from a pork sample.

The pork sample consists of a variety of different pork tissue types, meat, fat and kidney. Each tissue type is approximately 1mm thick, and the area measured using THz is approximately $13x10mm^2$ with a 500μm step size. The temporal scan at each pixel was 10ps long, giving a frequency resolution of 100GHz, and each pixel took approximately 1 minute to measure. The sample was mounted on cellulose nitrate film and a 1mm thick polythene window, before being placed behind a THz radiation source (<110>ZnTe; 1mm thick, $20x25mm^2$). Details of the apparatus used to obtain the images will be described later with reference to Figures 18 to 26.

At each pixel, the tissue type was identified using both the change in the magnitude and temporal position of the electric field maximum. All tissue types were found to transmit THz pulses, with the absorption increasing in the order: fat, meat, and kidney. The THz image shown in Figure 3(b) is a panchromatic THz image since the analysis of the absorption was not frequency specific.

Comparing the visible and THz images, the different tissue types have been successfully imaged and identified at THz frequencies. Due to the simplistic nature of this analysis there is an increased error along the boundary of each tissue region due to some scattering, which results in tissue types being incorrectly identified in these regions. Figure 4 shows power spectra for each tissue type . The data was taken at 3 different pixels. Clear differences in the absorption characteristics for each tissue type are shown.

Figure 5 shows data of the absorption coefficient for skin and kidney using the attenuation of the peak of the THz electric field. All samples were dried to minimise water absorption effects in the data. The data illustrates that the absorption coefficients for the two tissue types are different, which may be used to identify the tissues in an image; the thickness can be found from the temporal shift. Thus, the maximum tissue thickness that can be measured assuming a signal to noise ration (SNR) of 10^4:1. For this example, these values are 3.0mm for kidney and 7.5mm for skin. With the addition of an amplifier to boost visible, and hence THz, powers 10^5:1 - 10^6:1 can be achieved, which allows several cm of tissue to be probed in theory.

Figure 6 shows data from six types of chicken tissue: bone, cartilage, skin (cooked and uncooked), meat (cooked and uncooked). All tissue types were found to transmit THz by varying amounts. The meat has the strongest absorption of all the tissue types, with the electric field results multiplied by five for clarity. The frequency domain data (NH5) shows a clear difference in the nature of the absorption for each type of tissue.

Figure 7 shows the data from Figure 6 plotted on a single axis for comparison.

THz can be used to image the contents of objects that are otherwise opaque at particularly visible wavelengths, much in the same way as x-rays are currently used. However, due to the non-ionising nature of THz plus the low average powers, THz is inherently safe. For example, common packaging materials such as plastics, paper and

cardboard have been found to be transparent at THz frequencies. Figure 8 shows a visible image of a spider mounted over a hole in a metal plate. The spider is placed in a plastic box for imaging as shown in Figure 9a. At visible wavelengths it was not possible to observe the contents of the plastic box with the lid closed, Figure 9b.

The spider and the box were imaged over a 10x10 mm region with a 200μm step size. Analysing the image using the change in peak of the THz electric field, a THz image was formed of the contents of the box, Figure 10. The light areas correspond to regions of highest THz transmission. The spider is clearly resolved inside the box, with fine detail, such as a break in one of legs (top right corner) resolvable. Closer inspection of the Figure 10 also revealed some weak internal structure inside the spider.

Of considerable interest to medical applications would be the ability to measure the properties of blood using a non-invasive method on a human subject, i.e. a "contactless" in vivo method of assessing the constituents of the subject's blood. Thus, a technique that combines imaging and spectroscopic capabilities to locate and identify, respectively, different tissue types and their constituents would be of enormous medical and commercial value. Also, for imaging purposes blood is (partially) transmitting at THz frequencies. A sample of dried blood (black pudding) was taken and a thin layer spread on a piece of cellulose nitrate film. The transmission was measured at a single point on the sample, Figure 11a, with the peak electric field decreasing by 55%. In the frequency domain, Figure 11b, the absorption is found to be strongest between 1.00THz and 1.90THz, with a strong absorption around 0.66THz.

One of the most important materials that must be considered for biological applications of THz is liquid water. Water is known to have a number of strong absorption bands in the infrared and far-infrared/THz regions due to the polar nature of the molecule, and ultimately it may be absorption due to liquid water in biological samples that limits the applications of THz technology. To quantify the strength of water absorption a thin (90μm) layer of liquid water was measured. This layer was

formed on the surface of a piece of cellulose nitrate film. The time-domain results for the sample and a reference (dry cellulose nitrate) are shown in Figure 12a, and the frequency domain results in Figure 12b. From the time-domain results alone the absorption is clearly stronger than in the blood sample. Considering the frequency domain results, the absorption is found to increase with increasing frequency; at frequencies above 2.5THz the repeatability of the spectra is less reliable and therefore only the frequency range 0.6THz to 2.5THz should be examined. It is therefore important for biological applications that the frequency range of THz spectroscopy is extended to higher and lower frequencies where absorption windows are present. It should be noted, however, that the ability of THz to probe the skin, blood, and water thicknesses noted above suggests that it is possible to use the present invention.

In Figures 14 a to c, a commercially available, discrete transistor was taken which has the active elements encapsulated in a black casing that is opaque at visible wavelengths, Figure 13a. Fortunately, because the black casing is partially transparent to THz, the internal structure of the device can be imaged. The THz image in Figure 13b was constructed using 150μm steps over a 5x6mm^2 region centred on the transistor. Where there is only plastic, THz pulses are transmitted, but where there are metal tracks of the three leads, no THz is transmitted. To confirm the accuracy of the THz image, an identical transistor was cut open and the same lead arrangement was found, as recorded in the visible photograph of Figure 13c. Additional information on the depth of the leads below the outer surface could be obtained using reflection-based imaging. Scanning the THz beam across the front of the sample, strong reflections were recorded in regions with the metal tracks, with the temporal delay of the pulses giving the distance of the tracks below the surface.

A simple image of the distribution of the doping in a semiconductor can be formed using the change in the peak of a transmitted THz pulse, due to the approximately linear increase of THz free-carrier absorption with carrier density. Figure 14b shows a visible image of a sample consisting of two strips of undoped GaAs and two strips of n-type ($n \sim 1 \times 10^{18}$ cm^{-3}) with the strips arranged alternately side by

side. Each strip was 10x1x0.5mm. An area of approximately $8x8mm^2$ was imaged using THz, with a 200μm step size. While at visible wavelengths there was no means of identifying the GaAs, the THz image clearly shows a difference in the absorption, Figure 14a. Here the peak of the THz field is plotted for each pixel. The highest transmission (at the bottom of the image) is where there was no GaAs present. Moving across the GaAs strips there is variations in the absorption due to the different dopings, with absorption strongest in the n-type strips. Strip #3 also shows a step in the absorption at the boundary of the etch through the n-type doping.

Figures 16 and 17 show frequency dependent (monochromatic) images derived from the THz data of the semiconductor sample. Instead of plotting the peak of the field, power spectrum for each pixel is found using a fast Fourier transform and the power at a given frequency selected. Figures 16 and 17 show the images for f=2.38Thz and f=890Ghz respectively. At 2.75 THz the image is similar to Figure 14a, with the difference in the absorption between the two type of GaAs clearly resolvable. However, for the 890GHz image there is no difference in the transmission for the undoped and areas with no sample, with both appearing as "red" indicating that no absorption in the GaAs at this frequency.

Figure 18 shows a basic THz imaging system. The system can be simplified into three main sections, a generator 31, an imaging section 33 and a detection section 35. THz radiation is generated in the generating section 31 by using a THz emitter which is supplied by a visible pulsed laser 37.

A THz beam 39 is emitted from generation section 31 and is directed onto sample 41 of the imaging section 33. The THz beam 39 is then directed via further optics 45 into the detection section 35. The system of Figure 17 is an example of a near field imaging system, where the sample to be imaged is placed immediately behind the THz source.

The detection section reads the information carried in the detected THz signal via a visible light signal and AC Pockels effect. The visible light is ideally obtained from laser 37 via beam splitter 47. A time delay is added to the THz pulse via time delay line 34. The system (e.g. the control of the sample 41 movement, the time delay 34 and the detected signal processing) is controlled by computer 36.

Details of the AC pockels effect will be described with reference to Figure 19.

Figure 18 shows another imaging system. Here, for simplicity, details of the detection part of the system will be omitted. These will be described with reference to Figure 19.

The THz generation section is indicated by the components within box 51. The imaging system requires both a visible light pulse and a THz pulse to be emitted from the generation section 51. Therefore, the output coupler 23 should not 100% reflective to visible radiation to allow some visible radiation to be emitted from the THz generation section 51.

The emitted THz beam 53 and visible 55 from the generation system are incident on beam splitter 57. This beam splitter 57 allows transmission of the THz beam 53 but reflects the visible light beam 55 onto mirror 59 which reflects the beam 55 into optical delay line 61. The delayed beam 55 is then inputted into the THz detection unit 63.

The THz beam 53 is directed into the imaging section 52 and onto sample 65 via THz imaging optics 67. The sample 65 is located on a motorised X-Y translation stage (not shown) so that the whole sample 65 can be imaged. (The x-y plane is orthogonal to the beam axis). The THz radiation 69 carrying the imaging information from the sample is reflected into the THz detection system 63 via THz imaging optics 71.

The presence of visible radiation 55 as well as THz radiation 69 allows for imaging and electro-optic detection to be performed inside a single nitrogen-purged unit.

The sample 65 is mounted on a X-Y motorised translation stage (not shown) which is controlled by a PC computer (not shown). Each section (pixel) of the object may then be imaged. To improve the spatial resolution of the technique, off-axis parabolic mirrors, condenser cones, and lenses may be used to focus the beam to a diffraction limit spot. By mounting the sample in the near field of a condenser cone, the diffraction limit may be overcome and spatial resolution of about 50 μm may be achieved. The imaging system can function with or without such objects depending on the nature of the object to be imaged and the nature of the detection circuit.

Figure 19 shows the detection system in detail. The THz beam 69 carrying the imaging information and a visible light beam 55 are inputted into the THz detection system. The visible light beam 55 acts as a reference beam which is incident on the detection crystal 73. The reference beam 55 is linearly polarised and the polarisation is orientated such that it has components along both the ordinary and extraordinary axis of the detection crystal 73. Each of the axes has distinct refractive indices n_o and n_e along the ordinary and extraordinary axis of the crystal 73 respectively. In the absence of a second (THz) radiation beam 69, the linearly polarised reference beam 55 passes through the detection crystal 73 with negligible change in its polarisation.

The applicant wishes to clarify that the angle Θ through which the polarisation is rotated by is negligible. However, the linearly polarised beam can become slightly elliptical. This effect is compensated for by a variable retardation waveplate, e.g. a quarter waveplate 81.

The emitted beam 77 is converted into a circularly polarised beam 83 using quarter wave plate 81. This is then split into two linearly polarised beams by a Wollaston Prism 79 (or equivalent device for separating orthogonal polarisation

components) which directs the two orthogonal components of the polarised beam onto a balanced photodiode 85. The balanced photodiode signal is adjusted using wave plate 81 such that the difference in outputs between the two diodes is zero.

However, if the detector 73 also detects a secondary beam 69 (in this case a beam with a frequency in the THz range) as well as a reference beam, the angle Θ through which the polarisation is rotated by is not negligible. This is because the THz electric field modifies the refractive index of the visible (fundamental) radiation along one of the axes n_e, n_o. This results in the visible field after the detector 73 being elliptical and hence the polarisation components separated by the prism 79 are not equal. The difference in the voltage between the output diodes gives a detection voltage.

The reference beam 55 and the THz beam 69 should stay in phase as they pass through the crystal 73. Otherwise the polarisation rotation Θ is obscured. Therefore, the detection crystal 73 has phase matching means to produce a clear signal.

All of the items shown in Figure 20 sit on an optical bread board of dimensions 36 inches by 36 inches. The only external units required are a power supply for the diode laser and a cooling unit for the generation section 51.

The imaging section 91, has a motorised stage which is movable in the x-y plane, i.e. along two orthogonal axis which are perpendicular to the incident beam of THz radiation.

The imaging section 91 has two mirrors M11 and M12. Mirror M12 directs the THz beam 53 onto the sample 65. Mirror M11 is positioned to reflect the THz radiation transmitted through sample 65 onto the detection crystal 73. Mirrors M11 and M12 are off axis parabolic (OAP) mirrors. Such mirrors are configured so that the phase difference between the incident and reflected beams is the same at all points on

the mirror. The parameters resulting in an off axis parabolic surface are characterised by the focal length of the mirror.

An optical delay section 93 is also shown. The visible light beam emitted from the generating section is reflected by beamsplitter 57 into delay section 93. The delay section 93 has a corner cube mirror M9 which is moveable along the beam axis. The beam is directed onto corner cube mirror M9 via mirror M8. The beam is reflected off corner cube mirror M9 onto mirror M10. Corner cube mirror M9 is oscillated back and forth along the beam direction with an oscillation frequency of several 10s of Hz. This increases or decreases the path length of the visible beam 55 as required. A Clark ODL-150 system may be used to drive the mirror, this is capable of delays of 150ps. The emitted beam is then combined with the emitted THz beam at mirror M11. Alternatively the THz and visible beams may be combined colinearly using a beam splitter, for example, a pellicle beam splitter. Such a device would be placed before or after M11 and would eliminate the requirement for a hole in M11.

Figure 21 shows a variation on the imaging section 91 of Figure 20. The extended path length over which the THz beam 53 travels is purged with nitrogen to remove water vapour and hence improve the quality of the image.

Due to diffraction effects associated with the large wavelengths in the THz range, the cross-sectional size of the THz beam 53 and imaging applications is not sufficiently large that it may be treated as plain parallel. If diffraction effects <u>are</u> such that the radiation is paraxial so that it can be represented by a scalar field distribution, Gaussian beam mode optics and optical techniques can be used. The simplest case for system design is to assume that the fundamental mode dominates the beam profile. The use of Gaussian mode optics and design applied to conventional THz radiation and systems (generated in the Fourier transform machines, far-infrared lasers or Gunn diodes) is applicable and important to THz imaging systems.

A number of design rules or guidelines should be followed when constructing a THz imaging system to obtain a good quality image. For transmission optics such as lenses, geometric losses are kept to a minimum by ensuring that the ratio of the lens thickness to focal length and diameter to focal length is less than 0.2. If this is satisfied, then losses in the lenses will be primarily due to absorption and reflection. In this case, choice of materials is important.

A requirement which arises in pulsed systems is the need for the material to be non-dispersive so that pulse broadening does not occur. Given these requirements, high density polyethylene (DHPE), polytetrafluorethylene (PTFE), high resistivity silicon (Si), and TPX are some of the best materials and can also be machined in a lathe; any material combining low absorption and low dispersion at THz frequencies is a good candidate for fabrication of transmission optics, provided its shape can be suitably fabricated for a lens. Reflection losses in lenses tend to be highly frequency dependent at THz frequencies. Therefore care must be taken in lens design to ensure that all frequencies across the pulse bandwidth undergo the same reflection (and absorption) losses.

Ideally, reflective optics (mirrors) are used wherever possible instead of transmission optics (lenses) in order to minimise a number of losses associated with transmission optics, which include (i) frequency-dependent reflection losses and amplitude pattern distortion at dielectric (e.g. air-lens) interfaces, (ii) frequency-dependent absorption losses, (iii) diffraction effects and distortions to field distribution due to power falling on the lens's surface at an angle.

An additional property of importance in imaging (and not particular to Gaussian mode beam optics) is that if two mirrors are separated by the sum of their focal lengths, then the size of the beam waist (minimum beam diameter in plane normal to optical axis) on the optical axis after the reflection from the second mirror will be frequency-independent. This is true of the last mirror (focusing element) in a chain provided there are an even number of focusing elements in the chain. This provides a major advantage

for THz imaging as the pulse is comprised of a wide range of frequency components, and it is desired to keep the object at a fixed position on the optical axis whilst images are being recorded at various (x, y) points and at all THz frequencies in the pulse. This is particularly important THz imaging as the spectral coverage (bandwidth) of THz pulses increases into the mid-infrared and even higher frequencies.

The system in Figure 21 will produce beams with 1/e diameters (for the fundamental Gaussian mode in the beam) of 1-2 mm at the sample in the THz frequency range (e.g. at 300GHz, diameter = 2mm). In the system of Figure 21, six mirrors and two lenses are used as opposed to the two mirrors of Figure 20. The direction of the beam in Figure 21 is reversed to that in Figure 20. In the imaging section, the beam is first reflected off first OAP mirror 101 onto second OAP mirror 103 and then onto third OAP mirror 105. Second 103 and third OAP mirrors each have a focal length of 250 nm. They are separated by 500 nm.

The beam is reflected from the third OAP mirror 105 onto plano-convex lens 107 which has a focal length of 10 mm and a diameter of 10 mm. Third OAP mirror 105 is separated from plano convex lens 107 by 260nm (i.e. the sum of their focal lengths). The lens 107 is made from polyethylene or high resistivity Si. The lens 107 is placed 10 mm from the motorised stage (not shown) on which sample 109 is mounted. The beam has traversed through an even number of focussing optics and mirrors (101, 103, 105 and 107) which are all spaced apart by the sum of their focal lengths. Hence, the waist of the beam at the sample is independent of the frequency. Here, the beam diameter is chosen to be 2 mm, independent of frequency in the frequency range of about 300 GHz (0.30THz).

Once the beam has passed through sample 65, the transmitted THz radiation falls onto second plano convex lens 111. Plano convex lenses 107 and 111 are identical in optical characteristics. Lens 111 focuses the THz radiation onto the fourth OAP mirror 113. Fourth OAP mirror 113 has a focal length of 250 mm and reflects the THz beam onto fifth OAP mirror 115. Fifth OAP mirror 115 also has a focal length of 250

mm and lies 500 nm away from the fourth OAP mirror 113 (i.e. the sum of the focal length of the fourth and fifth OAP mirrors).

The beam is reflected from the fifth OAP mirror 115 to the sixth OAP mirror 117. Sixth OAP mirror has a focal length of 30 mm and is located 280 mm away from the fifth OAP mirror (i.e. the sum of the focal length of the fifth and sixth OAP mirrors).

The sixth OAP mirror 117 is provided with a hole 119. The visible light beam 55 is passed through this hole to combine it with the THz beam 69 for detection.

Further improvements in spatial resolution may be achieved by inserting condenser cones (made of brass or copper, highly polished on insides, with electro-plating and/or gold/silver evaporated coating) adjacent to the sample to be imaged as shown in Figure 22. In Figure 22, condenser cones 121 and 123 are located on either side of the sample 125 between the sample 125 and plano convex lenses 127 and 129 respectively. The plano convex lenses are the same as those described with reference to Figure 21. They have a focal length of 10 mm and are placed 10 mm away from condenser cones 121 and 123. The cones have a typical entrance aperture of 2 mm and an exit aperture of between 50 to 100 μm.

The sample 125, is typically placed within a few wavelengths of the exit aperture of condenser cone 121 e.g. about 100 μm, such that near field imaging techniques may be used to realise THz spot sizes at the sample which are less than the diffraction-limited spot size.

Another advantage of this design is that the beam waist size is frequency independent at the aperture entrance, so that all frequencies in the pulse should fit into the condenser cone.

The plano-convex lenses 127, 129 condenser cones 123, 121 and sample 125 are placed between OAP mirrors 131, 133. The mirrors have a focal length of 250 mm. THz beam 53 is reflected from OAP mirror 131 onto plano convex lens 127 which focuses beam 153 onto condenser cone 121. The beam 53 enters through the widest aperture of the condenser cone and exits through the narrowest aperture onto sample 125. Once beam 53 has passed through sample 125 it enters condenser cone 123 and exits the condenser cone 123 through its narrowest aperture onto plano convex lens 129. The beam is then reflected off OAP mirror 133 onto the detection crystal 73. The OAP mirror 133 has a hole 135. Visible light from the generator is combined with the THz beam 69 at mirror 133. It should be noted also that the optical configuration in Figure 7 can also be used with a multiplicity of other mirrors, such as the arrangement in Figure 21. It should be noted, however, that a variety of different focal lengths are possible for mirrors 133 and 131.

Also, the arrangement of condenser cones used here can easily be inserted into the system of Figure 21 using similar guidelines to beam size and mirror placement as those already elucidated.

It should be noted that simpler coupling systems such as that in Figure 23 are possible which utilise only two off-axis parabolic mirrors. These reduce the path length of the beam and therefore minimise losses due to any water vapour or other absorbing gases in the beam path. However, transmission optics are necessary in order to create frequency independent beam waists at the same and/or to realise higher spatial resolution.

In Figure 23, the THz beam 53 is reflected from OAP mirror 141 onto sample 143. The focal length of OAP mirror 141 is 30 mm and sample 143 is placed 30 mm away from OAP mirror 141. Optionally, further optical components such as lenses and condenser cones as described in Figure 22 may be added between mirror 141 and sample 143.

Once beam 53 has passed through sample 143 it is encoded with imaging information and is referred to as beam 69. Beam 69 is reflected from OAP mirror 145 onto the detection crystal. The OAP mirror is provided with a hole 147 which allows the visible beam 55 to be mixed with the THz beam 69 for detection.

Figure 24 shows a further example of an imaging system. The details of these components will not be repeated here. In Figure 24, the delay section of Figure 20 is replaced with a grating pair or an optical fibre 151 which chirps the visible pulse, extending its temporal width from 50 fs to about 20 ps. The different wavelength components in the visible pulse travel through the detection crystal 73 at different times.

Thus, when a grating spectrometer 153 is used to spatially disperse the wavelengths and a CCD camera 155 is used to record the spatial diversion, each pixel in the (for example) X-direction corresponds to a different wavelength and hence a different time. The result is that a given row of pixels in the x-direction on the CCD 155 effectively map out the temporal form of the THz beam which co-propagates through the detector crystal 73 and rotates the polarisation of the visible beam at different times during the pulse by varying amounts. Thus, transmission through the object being imaged is plotted as a function of time along one direction in the CCD array. Hence, the rotation of the polarisation of the reference beam 55, is measured by crossed polarises 161, 163 which are arranged on either side of the detection crystal 73.

The imaged object may then be stepped in the y direction on the translation stage in the usual way to develop a 2D THz image. Alternatively, if the probe beam is focused down by a cylindrical lens to a line (say 400 μm in x by 10mm in y) on the sample, the THz transmission along the y axis of the sample can be measured by the pixels along y direction of the CCD, i.e. the y-pixels of the CCD may then be used to image the object in the y-direction without resorting to the translation stage moving in y. A full image is then completed by stepping the translation stage in x. Both of these abilities (to measure time delay along the x-axis of the CCD and y image information

without mechanical movement) resulting in much quicker acquisition times if sufficient THz power is available as in this intra-cavity design to affect higher signal to noise ratios. Quicker data acquisition and potentially cheaper cost for more compact systems are the result.

The primary advantage of this system is the fast data acquisition owing to the lack of moving parts such as translation stages; using this system, both a) imaging along the y-direction of the object and b) the sampling of the time domain is very fast, limited the creation of a time delay are very fast, limited only by the speed of the CCD camera and the need to average many frames from the camera to get adequate signal to noise rations (SNR) on the images. The latter is the chief mechanism which limits the application of this technique, and hence the realisation of real-time imaging. Poor SNR results in part from the fact that the balanced photodiode detection scheme outlined in Figure 5 can no longer be used because the quarter wave plate would introduce background light onto the CCD as strong as one-half of the total probe power. Small signal detection in this scenario will be overwhelmed by photon shot noise if a CCD camera is used. To reduce the "ambient" light level on the camera, crossed polarizers are used in which the signal on the CCD falls to zero in the absence of a THz electric field. Such as detection system is optimal for a CCD, but still does not provide as high signal-to-noise as the system in Figure 5, especially if lock-in detection is used in the latter case.

To overcome this SNR problem, regenerative amplifiers are used (not shown) to boost the optical peak power which nonlinearly generates the THz pulse, resulting in a larger THz field. Such a system suffers, however, from numerous disadvantages. Regenerative amplifiers are extremely expensive (~£100K) and tend to be large and bulky. Also, a second pump laser to drive the amplifier is required. Lastly, such systems operate at low repetition rates (50Hz-250kHz), resulting in a relative decrease in average power. The bright intracavity sources designed here would overcome all of these disadvantages. The intracavity design could therefore be a major step forward in the realisation of a THz imaging system with sufficiently quick data acquisition at

sufficiently high signal to noise ratios to realise THz images at video frame rates (~38 frames/sec), so-called "THz movies".

Figure 25 shows a further example of the imaging system of Figure 24. In Figure 25, the motorised stage (of Figure 24) is redundant. Instead, the imaging area of the CCD camera 155 is matched to the imaging area of the detection crystal 73. This area is typically several mm^2. The reference beam 55 is expanded by optics 170 (e.g. telescopic or analogous optics), such that the reference beam has a larger cross sectional area than the THz beam and ideally fills all the pixels in the CCD camera 155. The distribution of the rotated polarisation of the reference beam in the x-y plane (proportional to the THz power transmitted through the sample 65 in the x-y plane) is transferred to the pixels of the CCD camera, resulting in a THz image of the object appearing on a CCD or a computer screen (not shown) attached to the output of CCD camera 155. The time delay in this system is created by an optical delay line (as described with reference to Figure 20). This is the only mechanical moving part of the system.

CLAIMS:

1. A method of imaging a sample, the method comprising the steps of:

a) irradiating the sample to be imaged with pulsed electro-magnetic radiation with a plurality of frequencies in the range from 50 GHz to 84 THz;

b) subdividing an area of the sample which is to be imaged into a two dimensional array of pixels, and detecting radiation from each pixel over a plurality of frequencies; and

c) generating an image of the area of the sample from the radiation detected in step (b) using a frequency or a selection of frequencies from the plurality of frequencies in the pulsed electro-magnetic radiation.

2 A method according to claim 1, wherein the sample to be imaged is irradiated with pulsed electro-magnetic radiation with a plurality of frequencies in the range from 100 GHz to 20 THz

3 A method according to claim 2, wherein the sample to be imaged is irradiated with pulsed electro-magnetic radiation with a plurality of frequencies in the range from 500 GHz to 10 THz.

4. A method according to any preceding claim, wherein the input radiation is transmitted through the sample.

5. A method according to any of claims 1 to 3, wherein the input radiation is reflected from the sample.

6. A method according to any preceding claim, wherein the image is generated from a single frequency.

7. A method according to any of claims 1 to 5, wherein a single image is generated using a selected frequency range..

8. A method according to claim 7, wherein the selected frequency range is less than a third of the frequency range of the pulsed electro-magnetic radiation which irradiates the sample.

9. A method according to any preceding claim, wherein a plurality of images is generated from a corresponding plurality of different frequencies.

10. A method according to any preceding claims, wherein, in step (b), the radiation is detected in the time domain and is Fourier transformed to obtain frequency dependent data.

11. A method according to any preceding claim, wherein a fraction of the input pulsed radiation does not irradiate the area of the sample, which is to be imaged, and is detected as a reference signal.

12. A method according to any of claims 1 to 10 , wherein the method further comprises the step of detecting a reference signal when the area of the sample to be imaged is absent from the path of the pulsed electro magnetic radiation.

13. A method according to either of claims 11 or 12, wherein step (c) comprises the steps of deriving frequency dependent image data from the detected radiation and plotting the frequency dependent image data for each pixel to obtain an image of the sample.

14. A method according to claim 13, wherein step (c) further comprises the steps of calculating the Power Spectrum for the radiation detected in step (b) and calculating the Power Spectrum of the reference signal.

15. A method according to claim 14, wherein the frequency dependent image data is calculated by subtracting the Power Spectrum of the reference signal from the Power Spectrum of the radiation detected in step (b).

16. A method according to claim 14, wherein the frequency dependent image data is calculated by dividing the Power Spectrum of the radiation detected in step (b) by the Power Spectrum of the reference signal.

17. A method according to claim 13 , wherein the frequency dependent image data is calculated by deriving the frequency dependent absorption coefficient from a Fourier transform of the radiation detected in step (b) and a Fourier transform of the reference signal.

18. A method according to claim 13, wherein the frequency dependent image data is calculated by deriving the frequency dependent refractive index from a Fourier transform of the radiation detected in step (b) and a Fourier transform of the reference signal.

19. A method according to any of claims 13 to 18, wherein the frequency dependent image data is derived for two or more frequencies.

20 A method according to claim 19, wherein the frequency dependent image data for the two frequencies is added, subtracted, multiplied or divided for each pixel.

21. A method according to any preceding claim, wherein the frequency dependent image data is obtained for a narrow range of frequencies and the image data is integrated over this narrow range.

22. A method according to any of claims 13 to 21, wherein the frequency dependent image data is processed by subdividing the data into a plurality of bands, wherein each band represent a range of magnitudes of the image data for a single frequency or narrow frequency range and each band is assigned a single value or colour.

23. A method according to claim 22, wherein the bands are not of equal widths in magnitude.

24. A method according to either of claims 22 or 23, wherein the image data is derived for more than one frequency.

25. A method according to claim 24, wherein the image data for two frequencies is combined according to a predetermined rule.

26. A method according to claim 24, wherein there are two bands assigned the values '0' and '1' and the predetermined rule is a BOOLEAN algebraic rule.

27. A method according to any preceding claim, the method further comprising the step of displaying a sequence of images generated in step (c) for a plurality of different frequencies.

28. A method according to claim 27, wherein the image generated in step (c) is scanable through a continuum of frequencies.

29. A method according to claim 27, wherein the image generated in step (c) can be stepped through a plurality of discrete frequencies.

30. A method of imaging a sample, the method comprising the steps of :

a) irradiating the sample to be imaged with pulsed electro-magnetic radiation with a plurality of frequencies in the range from 50 GHz to 84 THz;

b) subdividing an area of the sample into a two dimensional array of pixels, and detecting radiation from each pixel over a plurality of frequencies; and

c) generating an image of the area of the sample from the radiation detected in step (b) by calculating the difference between the temporal positions of a maxima and a minima of the radiation detected in step (b) for each pixel.

31 A method according to claim 30, wherein the sample to be imaged is irradiated with pulsed electro-magnetic radiation with a plurality of frequencies in the range from 100 GHz to 20 THz.

32. A method according to claim 31, wherein the image is generated by calculating the difference between the temporal positions of the main minimum and maximum peaks.

33. A method according to any of claims 30 to 32, wherein step (c) further comprises the step of multiplying the difference between the temporal position of the maxima and minima, by a magnitude of the radiation.

34. A method according to claim 33, wherein the magnitude of the radiation is the difference in magnitude between the minimum and maxima of the detected radiation.

35. A method according to claim 33, wherein the magnitude of the radiation is the minimum or maximum of the detected radiation.

36. A method of imaging a sample, the method comprising the steps of :

a) irradiating.the sample to be imaged with pulsed electro-magnetic radiation with a plurality of frequencies in the range from 50 GHz to 84 THz;

b) subdividing an area of the sample into a two dimensional array of pixels, and detecting radiation from each pixel over a plurality of frequencies; and

c) generating an image of the area of the sample from the radiation detected in step (b) by calculating the difference between the magnitude of a maxima and a minima of the radiation detected in step (b) for each pixel.

37. A method according to claim 36, wherein the sample to be imaged is irradiated with pulsed electro-magnetic radiation with a plurality of frequencies in the range from 100 GHz to 20 THz

38. A method for imaging a sample, according to either of claims 36 or 37, wherein the peak minima and maxima are the main minimum and maximum.

39. An apparatus for imaging a sample, the apparatus comprising:

a) means for irradiating the sample with pulsed electro-magnetic radiation having a plurality of frequencies in the range from 50 GHz to 84 THz;

b) means for subdividing an area of the sample into a two dimensional array of pixels;

c) means for detecting radiation from each pixel over a plurality of frequencies; and

d) means for generating an image of the area of the sample from the detected radiation by using a frequency or a selection of frequencies from the plurality of frequencies in the pulsed electro-magnetic radiation.

40. An apparatus for imaging a sample, the apparatus comprising:

a) means irradiating the sample with pulsed electro-magnetic radiation having a plurality of frequencies in the range form 50 GHz to 84 THz;

b) means for subdividing an area of the sample into a two dimensional array of pixels;

c) means for detecting radiation from each pixel over a plurality of frequencies; and

d) means generating an image of the area of the sample from the detected radiation by calculating the difference between the temporal positions of a maximum and a minimum of the detected radiation detected for each pixel.

41. An apparatus for imaging a sample, the apparatus comprising:

a) means for irradiating the sample with pulsed electro-magnetic radiation having a plurality of frequencies in the range from 50 GHz to 84 THz;

b) means for subdividing an area of the sample into a two dimensional array of pixels;

c) means for detecting radiation from each pixel over a plurality of frequencies; and

d) means for generating an image of the area of the sample from the detected radiation by calculating the difference between the magnitude of a maximum and a minimum of the detected radiation for each pixel.

ABSTRACT:

Radiation Imaging

In an apparatus and method for imaging a sample:

a) the sample to be imaged is irradiated with pulsed electro-magnetic radiation with a plurality of frequencies in the range from 50 GHz to 84 THz;

b) an area of the sample is subdivided into a two dimensional array of pixels, and radiation from each pixel is detected over a plurality of frequencies; and

c) an image is generated from the radiation detected in step (b) using a frequency or a selection of frequencies from the plurality of frequencies in the pulsed electro-magnetic radiation.

(Fig. 17).

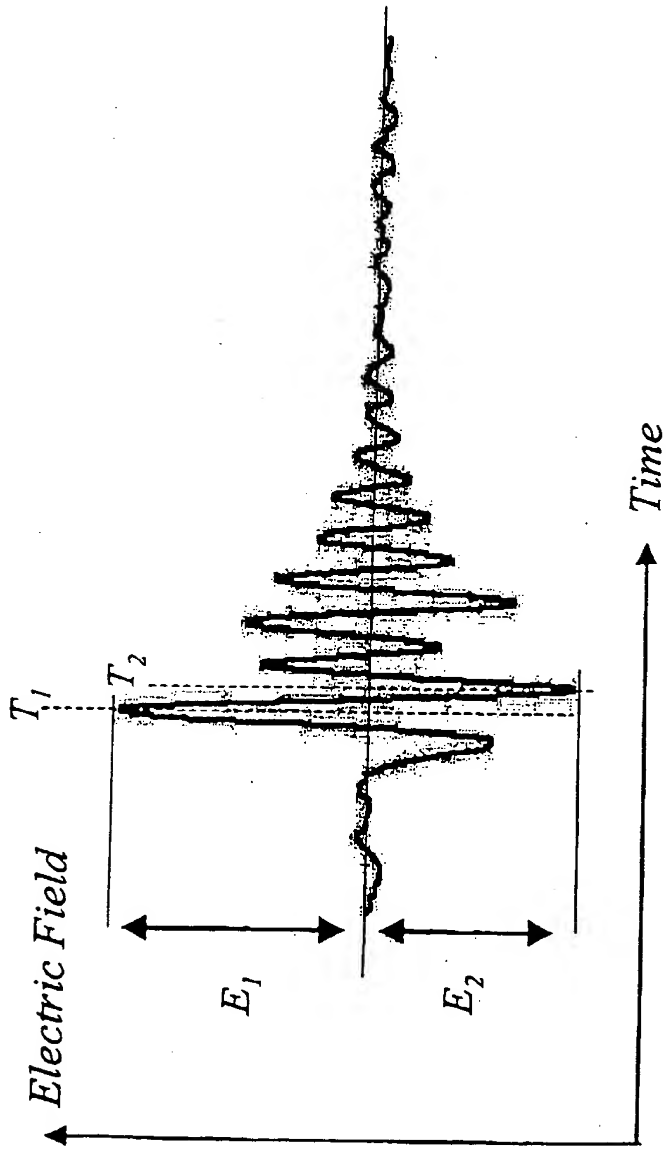

FIGURE 1

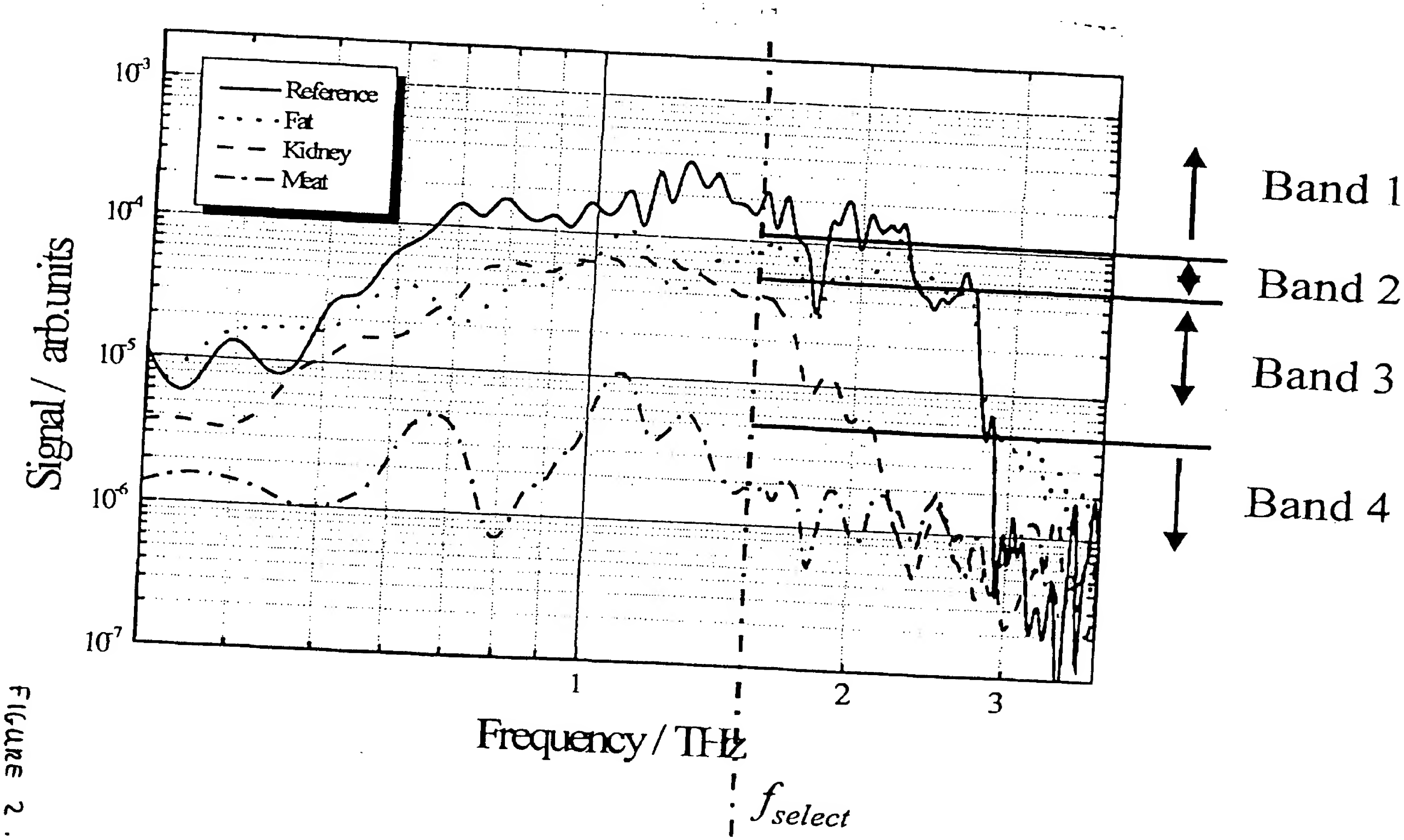
Reference
Fat
Kidney
Meat
Band 1
Band 2
Band 3
Band 4
10^{-3}
10^{-4}
10^{-5}
10^{-6}
10^{-7}
Signal / arb.units
1
2
3
Frequency / THz
f_{select}

FIGURE 2.

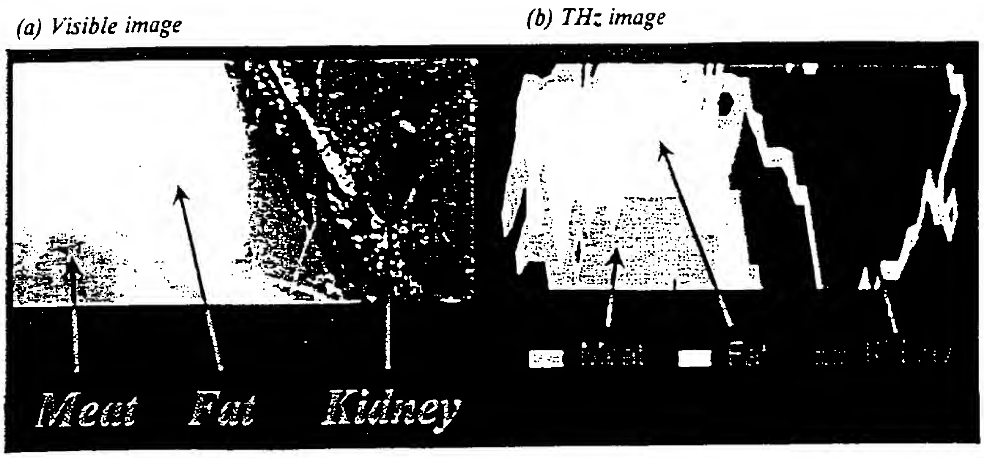

FIGURE 3

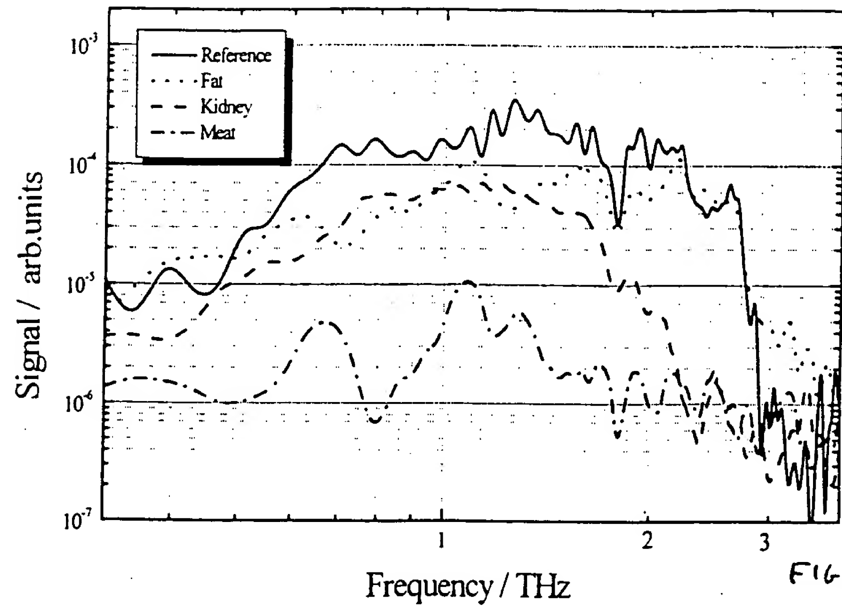

FIGURE 4

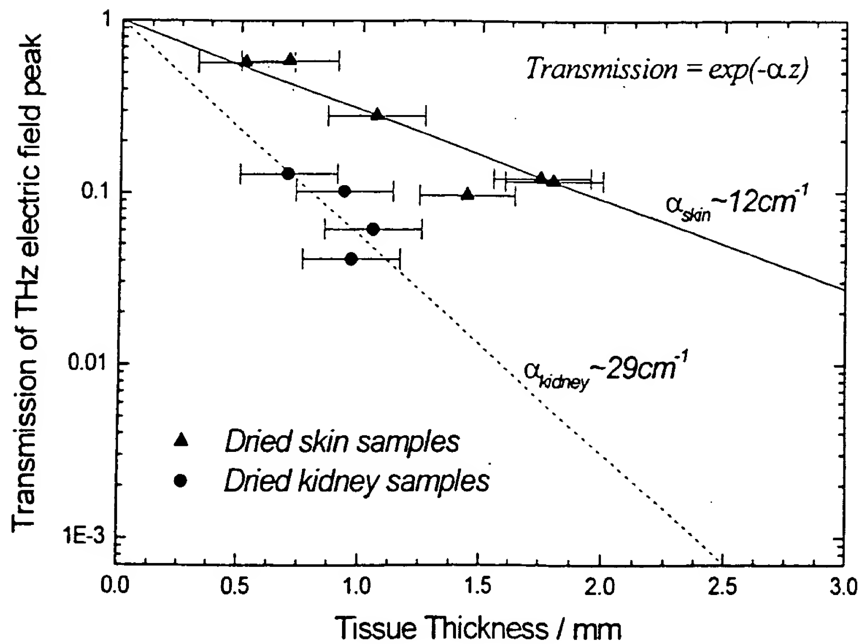

FIGURE 5

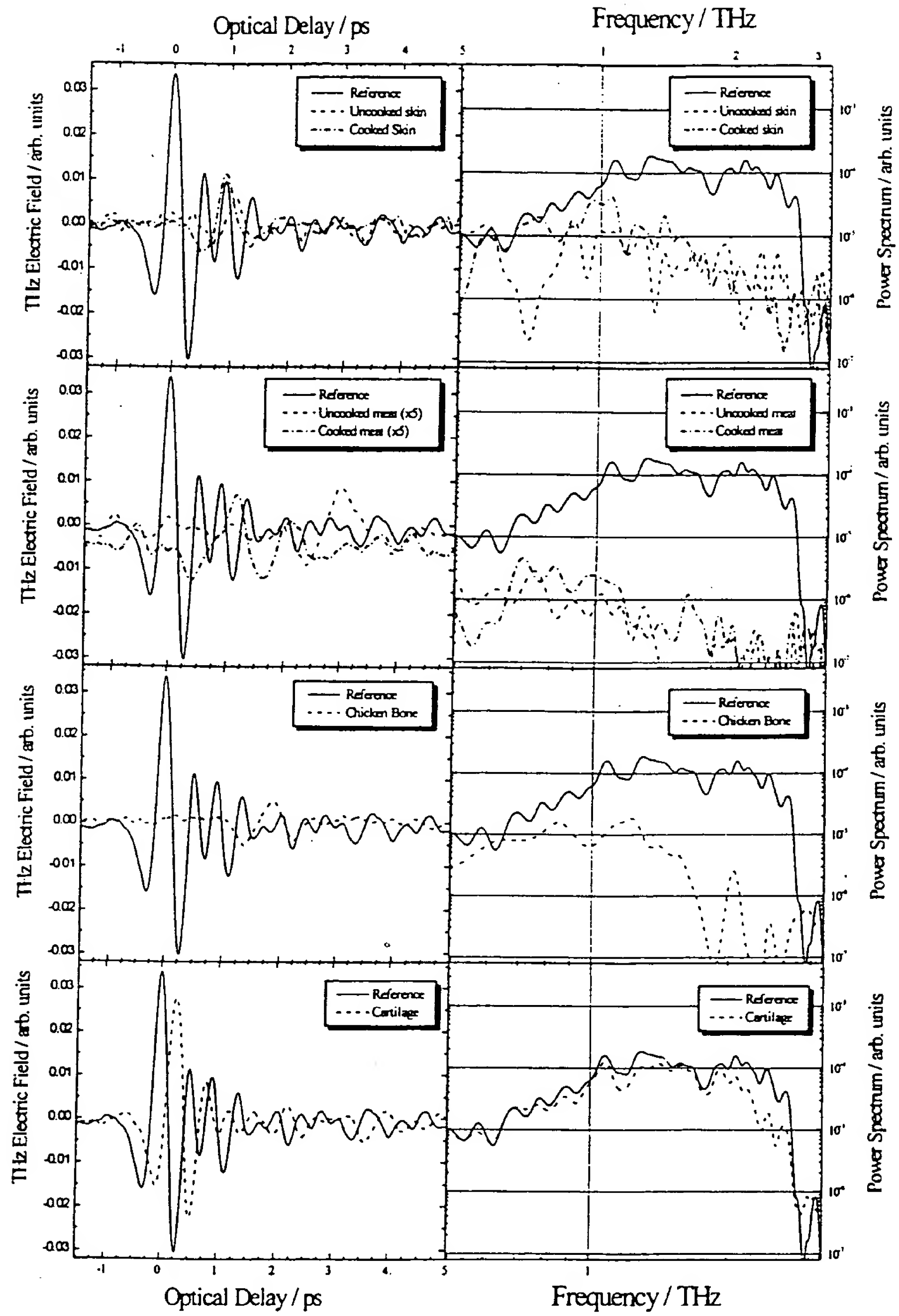

Optical Delay / ps
Frequency / THz
THz Electric Field / arb. units
Power Spectrum / arb. units
Reference
Uncooked skin
Cooked Skin
Uncooked meat (x5)
Cooked meat (x5)
Uncooked meat
Cooked meat
Chicken Bone
Cartilage

FIGURE 6

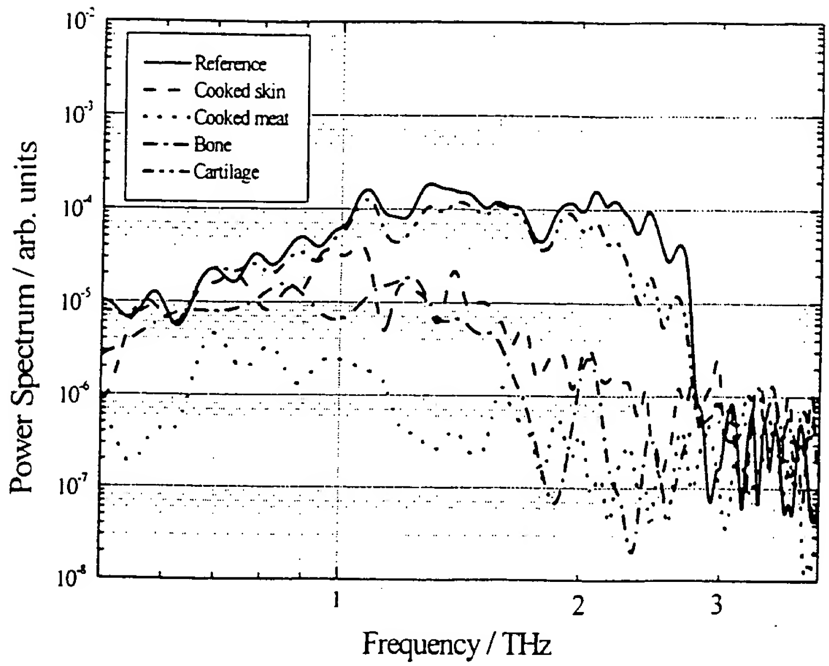

FIGURE 7

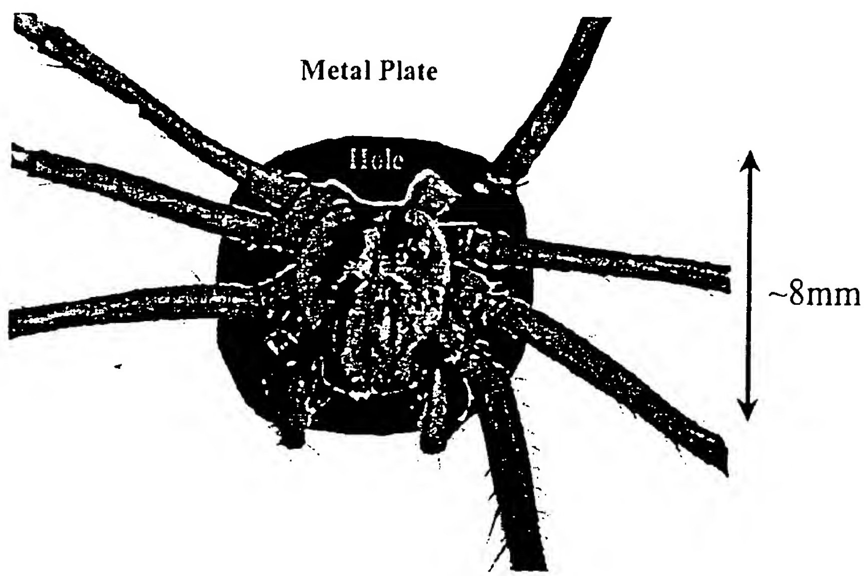

FIGURE 8

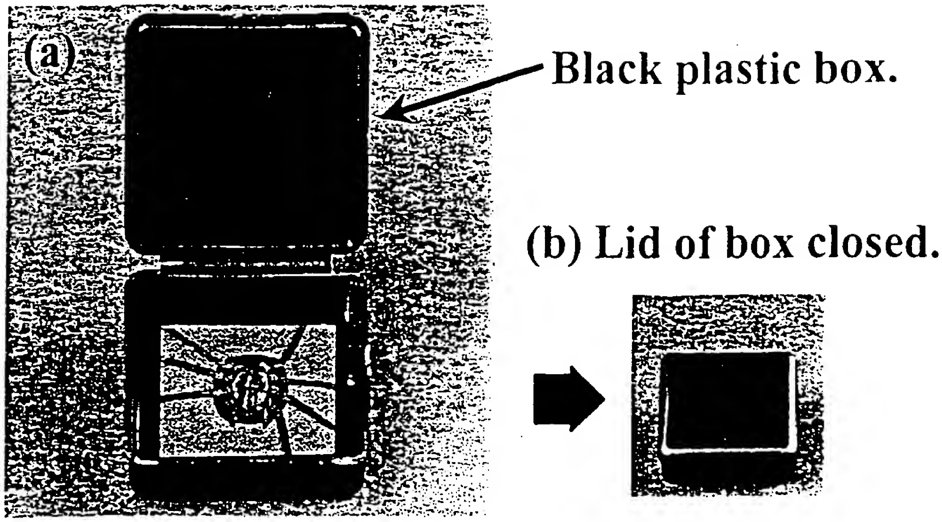

FIGURE 9

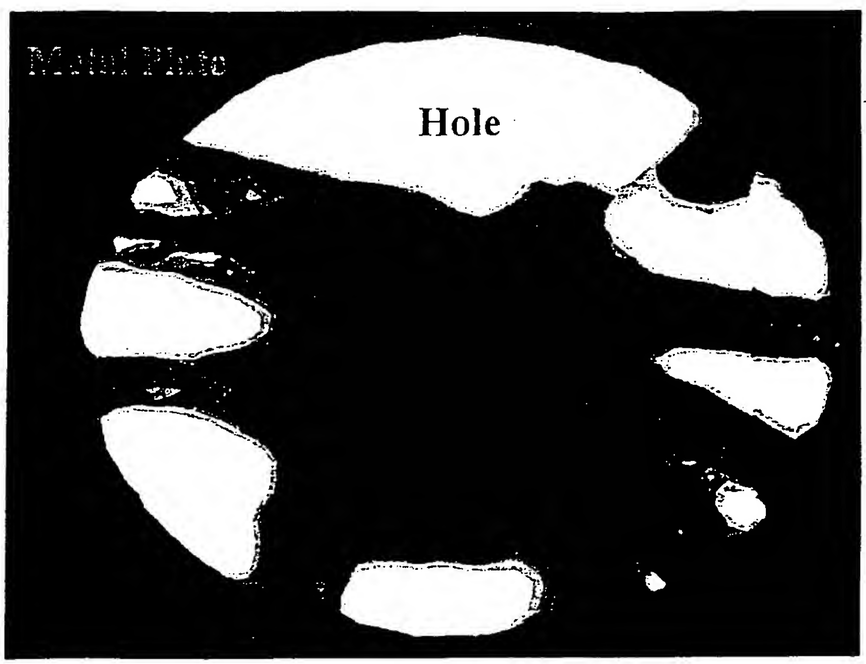

FIGURE 10

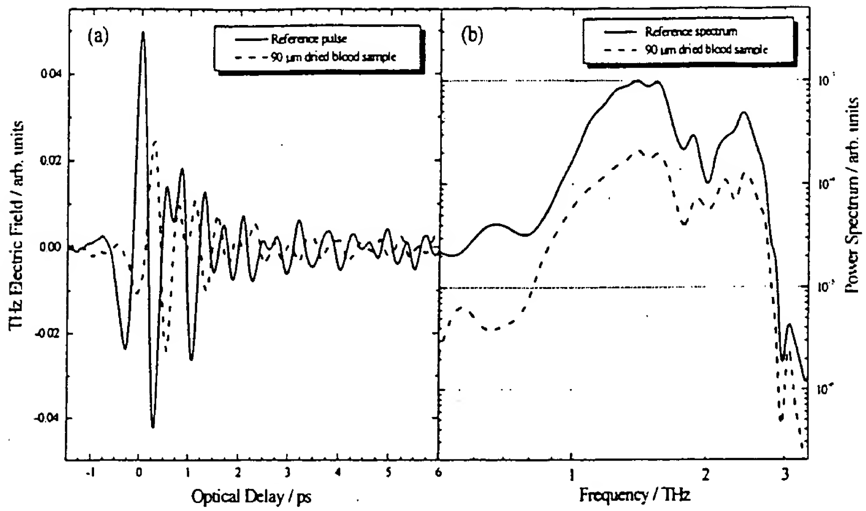

FIGURE 11

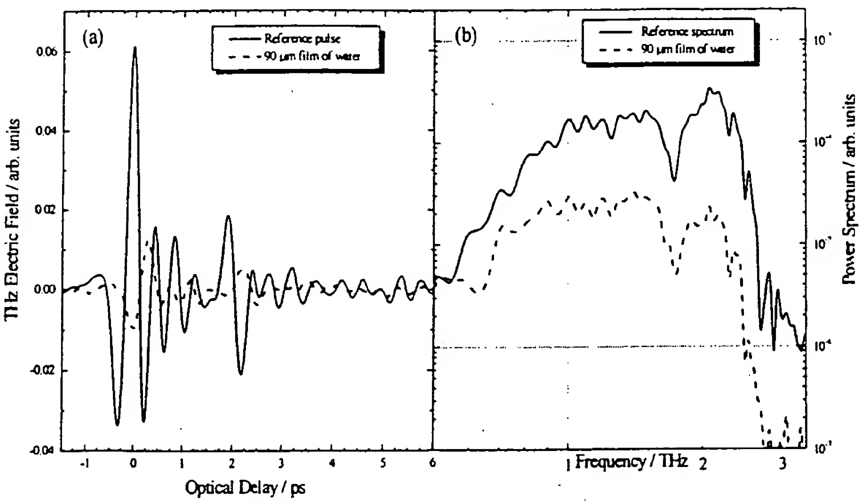

FIGURE 12

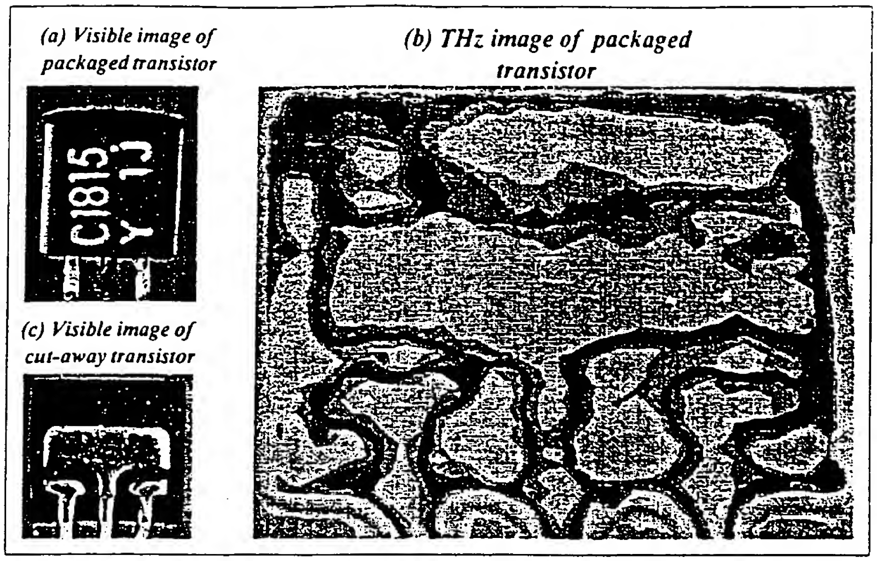

FIGURE 13

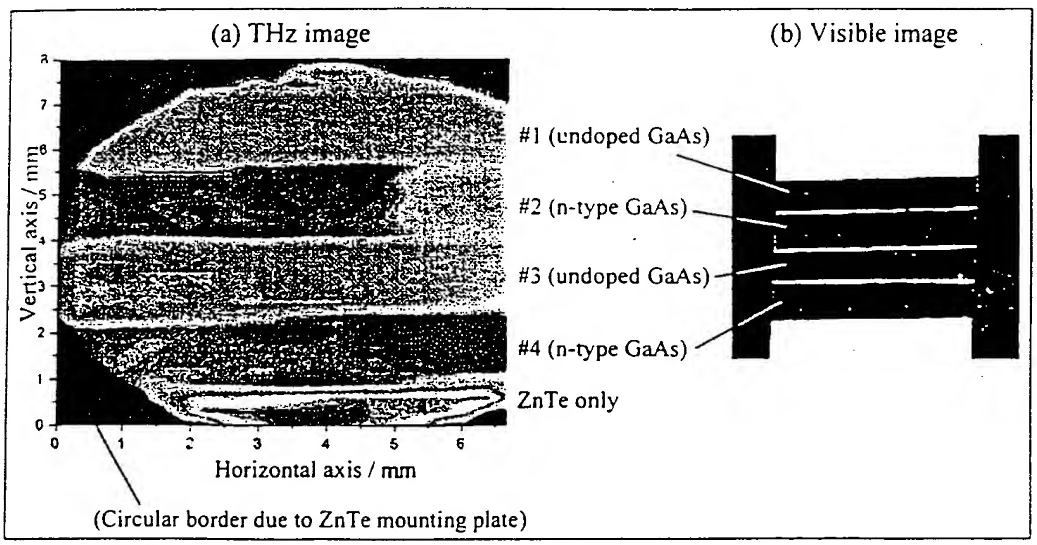

FIGURE 14

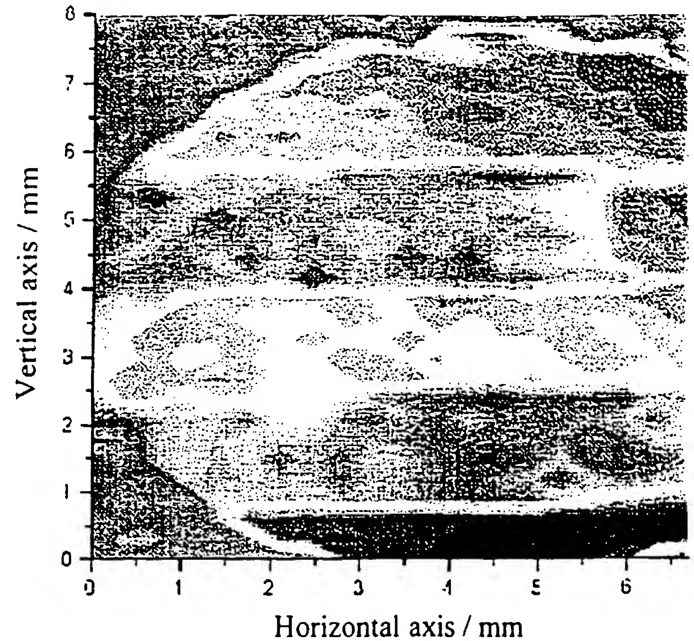

FIGURE 15

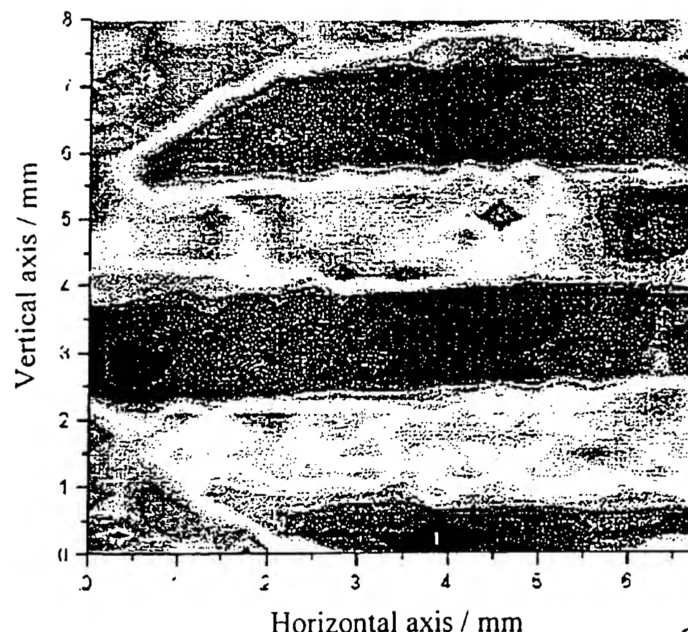

FIGURE 16

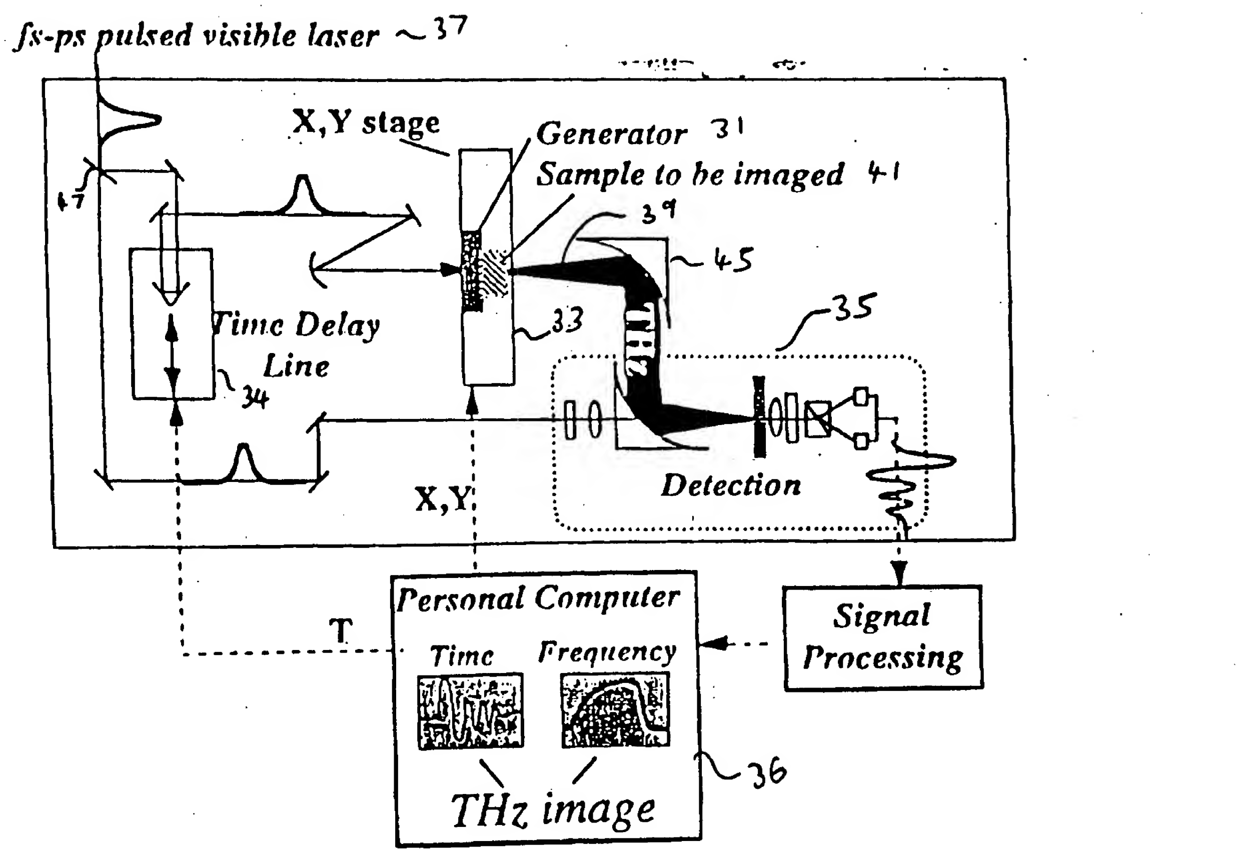
fs-ps pulsed visible laser 37
X,Y stage
Generator 31
Sample to be imaged 41
39
45
47
Time Delay Line
34
33
THz
35
Detection
X,Y
T
Personal Computer
Time
Frequency
THz image
36
Signal Processing

FIGURE 17

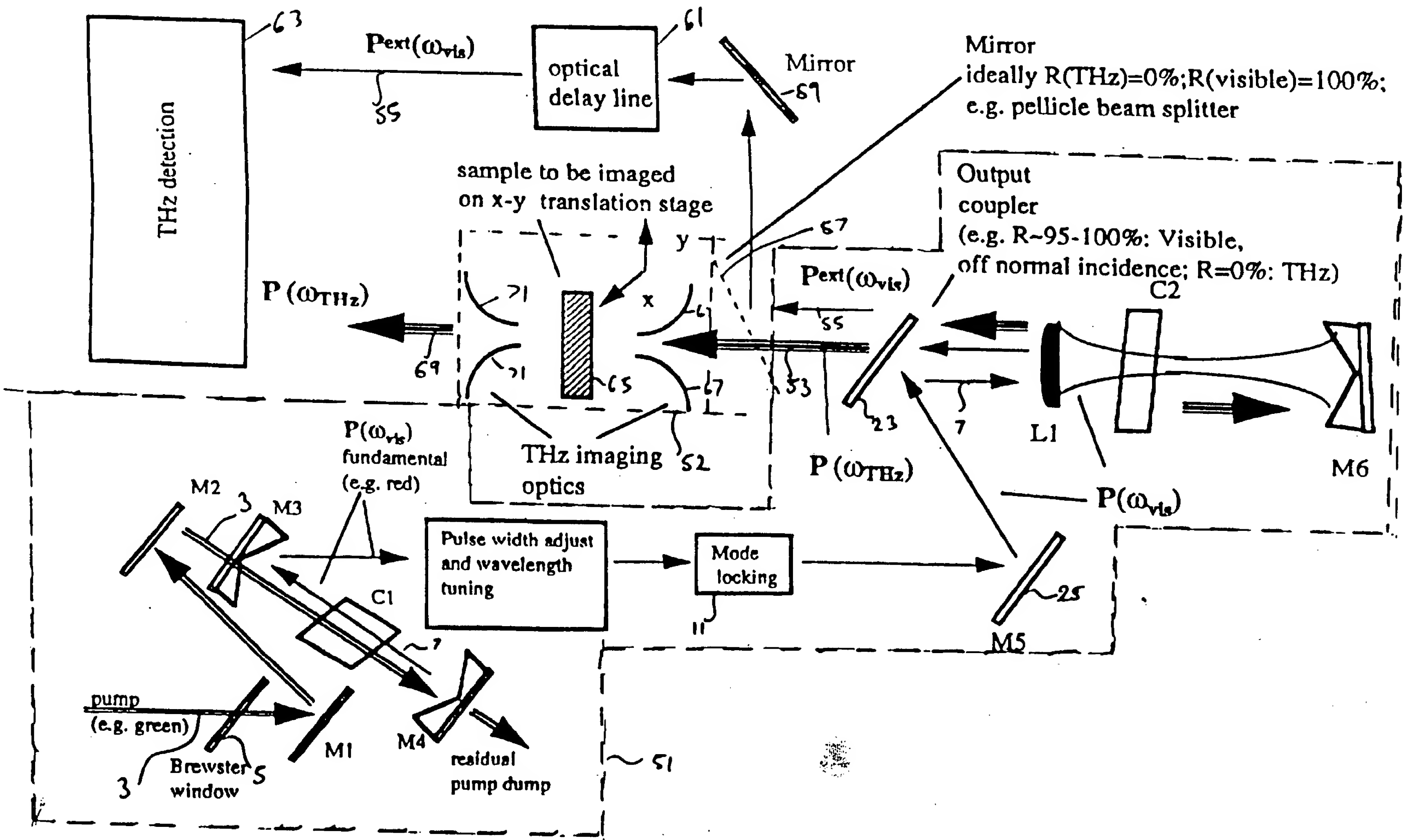
THz detection
63
Pext(ωvis)
55
optical delay line
61
Mirror
69
Mirror
ideally R(THz)=0%;R(visible)=100%;
e.g. pellicle beam splitter
sample to be imaged
on x-y translation stage
y
x
67
71
65
P (ωTHz)
69
Output
coupler
(e.g. R~95-100%: Visible,
off normal incidence; R=0%: THz)
C2
Pext(ωvis)
55
53
23
7
L1
M6
P (ωTHz)
P(ωvis)
P(ωvis)
fundamental
(e.g. red)
THz imaging
optics
52
M2
3
M3
C1
7
Pulse width adjust
and wavelength
tuning
Mode
locking
11
M5
25
pump
(e.g. green)
3
Brewster window
5
M1
M4
residual
pump dump
51

FIGURE 18

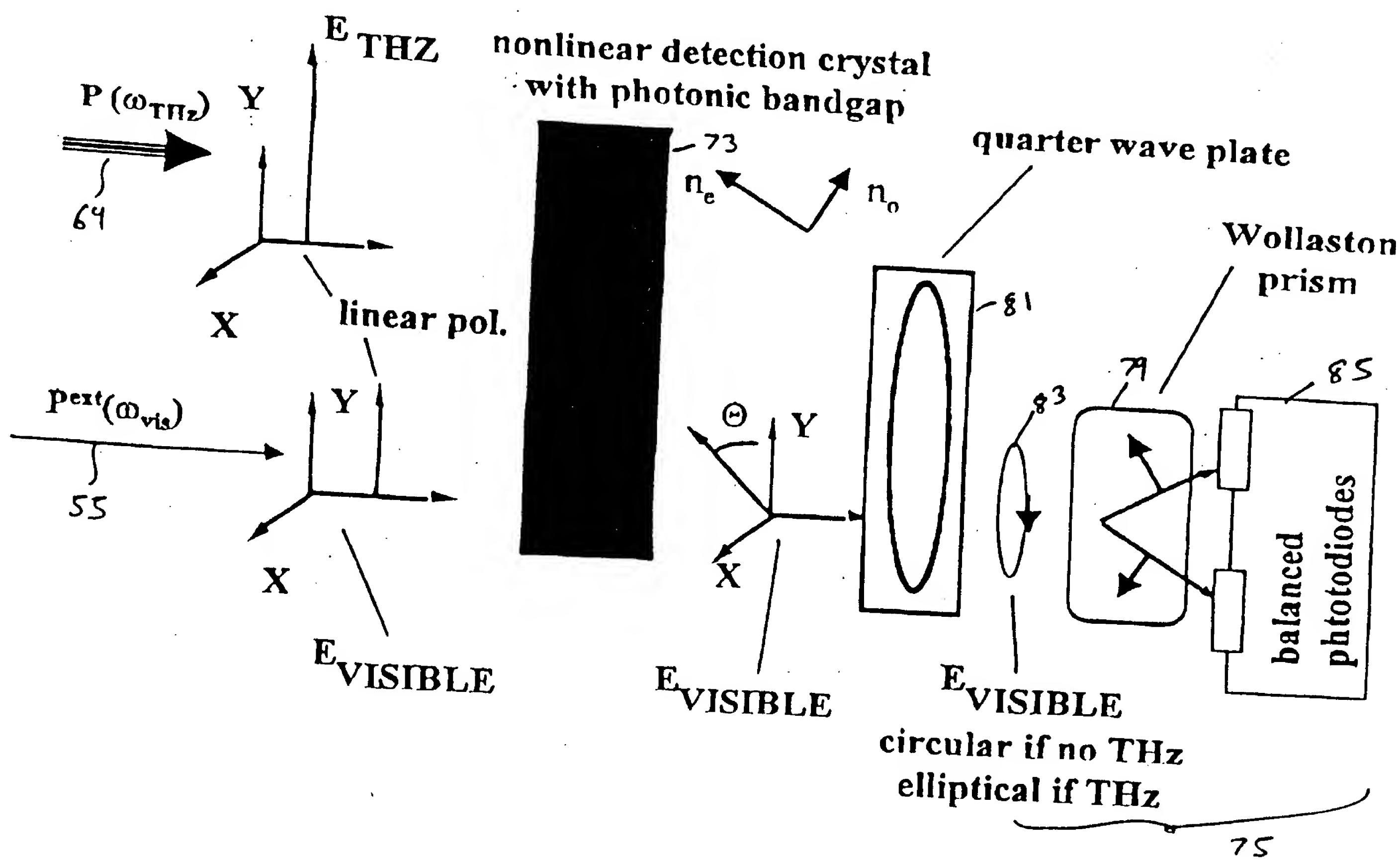

E THZ
P (ω_{THz})
Y
64
X
linear pol.
nonlinear detection crystal with photonic bandgap
73
n_e
n_o
quarter wave plate
81
Wollaston prism
79
85
$P^{ext}(\omega_{vis})$
Y
55
X
$E_{VISIBLE}$
Θ
Y
X
$E_{VISIBLE}$
83
$E_{VISIBLE}$
circular if no THz
elliptical if THz
balanced photodiodes
75

FIGURE 19

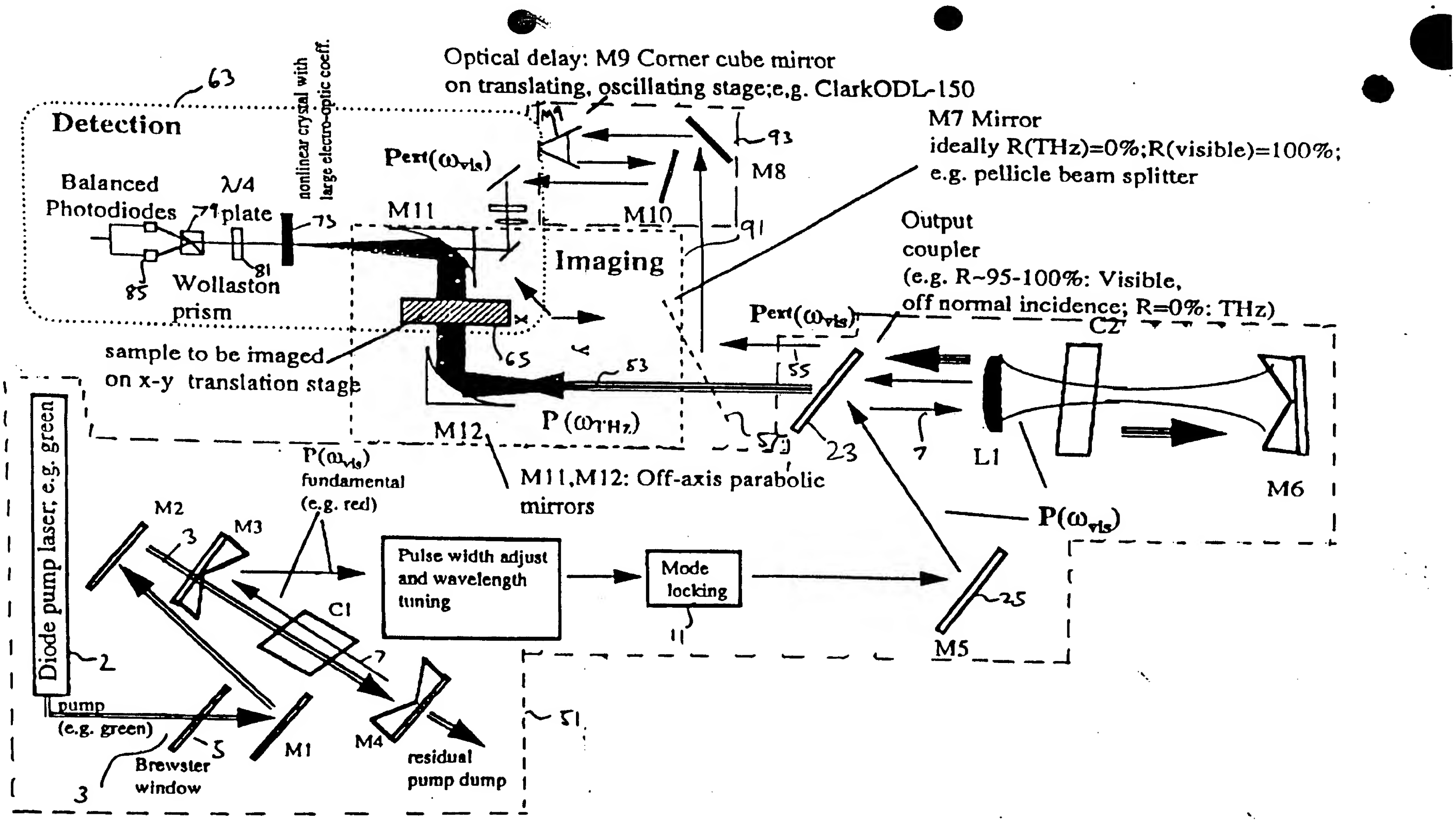

Optical delay: M9 Corner cube mirror
on translating, oscillating stage;e.g. ClarkODL-150
63
Detection
Balanced
Photodiodes
λ/4
plate
nonlinear crystal with
large electro-optic coeff.
Wollaston
prism
79
81
85
75
M9
93
M8
M10
91
M11
Pert(ωvis)
Imaging
M7 Mirror
ideally R(THz)=0%;R(visible)=100%;
e.g. pellicle beam splitter
Output
coupler
(e.g. R~95-100%: Visible,
off normal incidence; R=0%: THz)
C2
sample to be imaged
on x-y translation stage
65
x
y
53
55
57
23
7
L1
M6
M12
P(ωTHz)
P(ωvis)
fundamental
(e.g. red)
M11,M12: Off-axis parabolic
mirrors
P(ωvis)
M2
M3
3
C1
Pulse width adjust
and wavelength
tuning
Mode
locking
11
M5
25
Diode pump laser; e.g. green
2
pump
(e.g. green)
5
Brewster
window
3
M1
M4
residual
pump dump
51

FIGURE 20

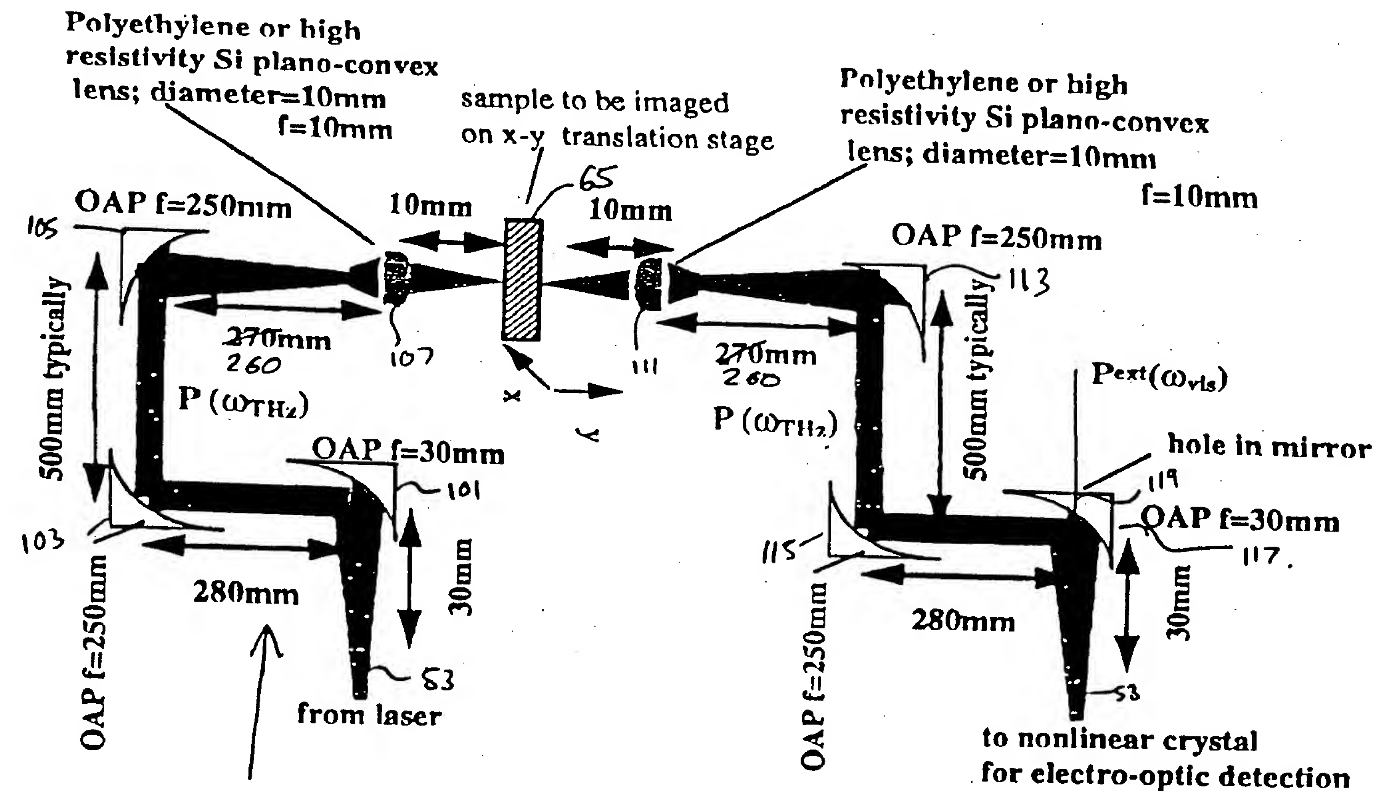

Polyethylene or high resistivity Si plano-convex lens; diameter=10mm f=10mm
sample to be imaged on x-y translation stage
Polyethylene or high resistivity Si plano-convex lens; diameter=10mm f=10mm
OAP f=250mm
105
10mm
65
10mm
OAP f=250mm
113
500mm typically
~~270~~mm 260
107
x
y
111
~~270~~mm 260
500mm typically
P (ω_{THz})
P (ω_{THz})
$P_{ext}(\omega_{vis})$
OAP f=30mm
101
hole in mirror
119
OAP f=30mm
103
115
117
280mm
30mm
OAP f=250mm
OAP f=250mm
280mm
30mm
53
from laser
53
to nonlinear crystal for electro-optic detection

FIGURE 21

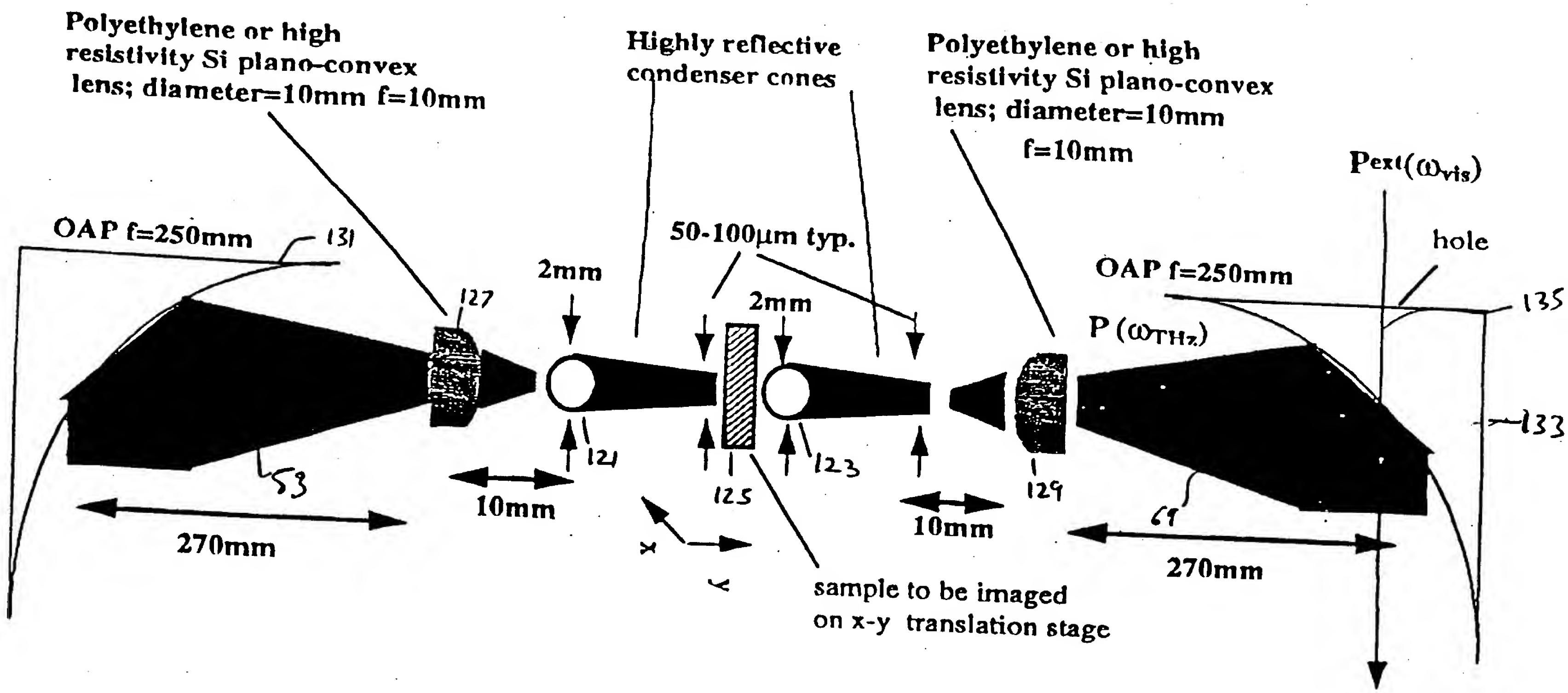

Polyethylene or high resistivity Si plano-convex lens; diameter=10mm f=10mm
Highly reflective condenser cones
Polyethylene or high resistivity Si plano-convex lens; diameter=10mm f=10mm
Pext(ωvis)
hole
OAP f=250mm
131
127
2mm
50-100μm typ.
2mm
OAP f=250mm
135
P (ωTHz)
121
125
123
129
133
53
10mm
10mm
69
270mm
x
y
sample to be imaged on x-y translation stage
270mm

FIGURE 22

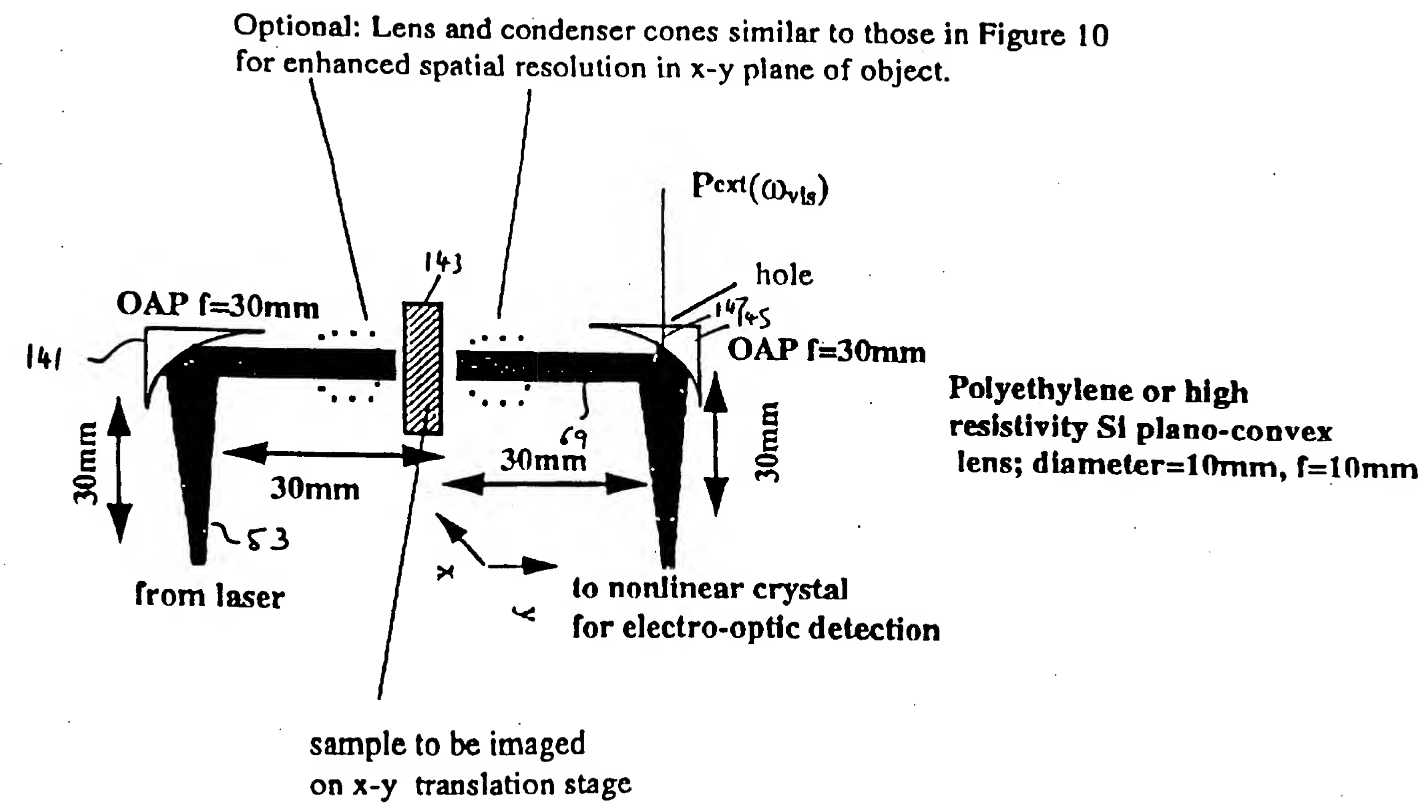

Optional: Lens and condenser cones similar to those in Figure 10
for enhanced spatial resolution in x-y plane of object.
Pext(ωvis)
143
hole
147
145
OAP f=30mm
141
OAP f=30mm
Polyethylene or high
resistivity Si plano-convex
lens; diameter=10mm, f=10mm
30mm
30mm
69
30mm
30mm
53
from laser
x
y
to nonlinear crystal
for electro-optic detection
sample to be imaged
on x-y translation stage

FIGURE 23.

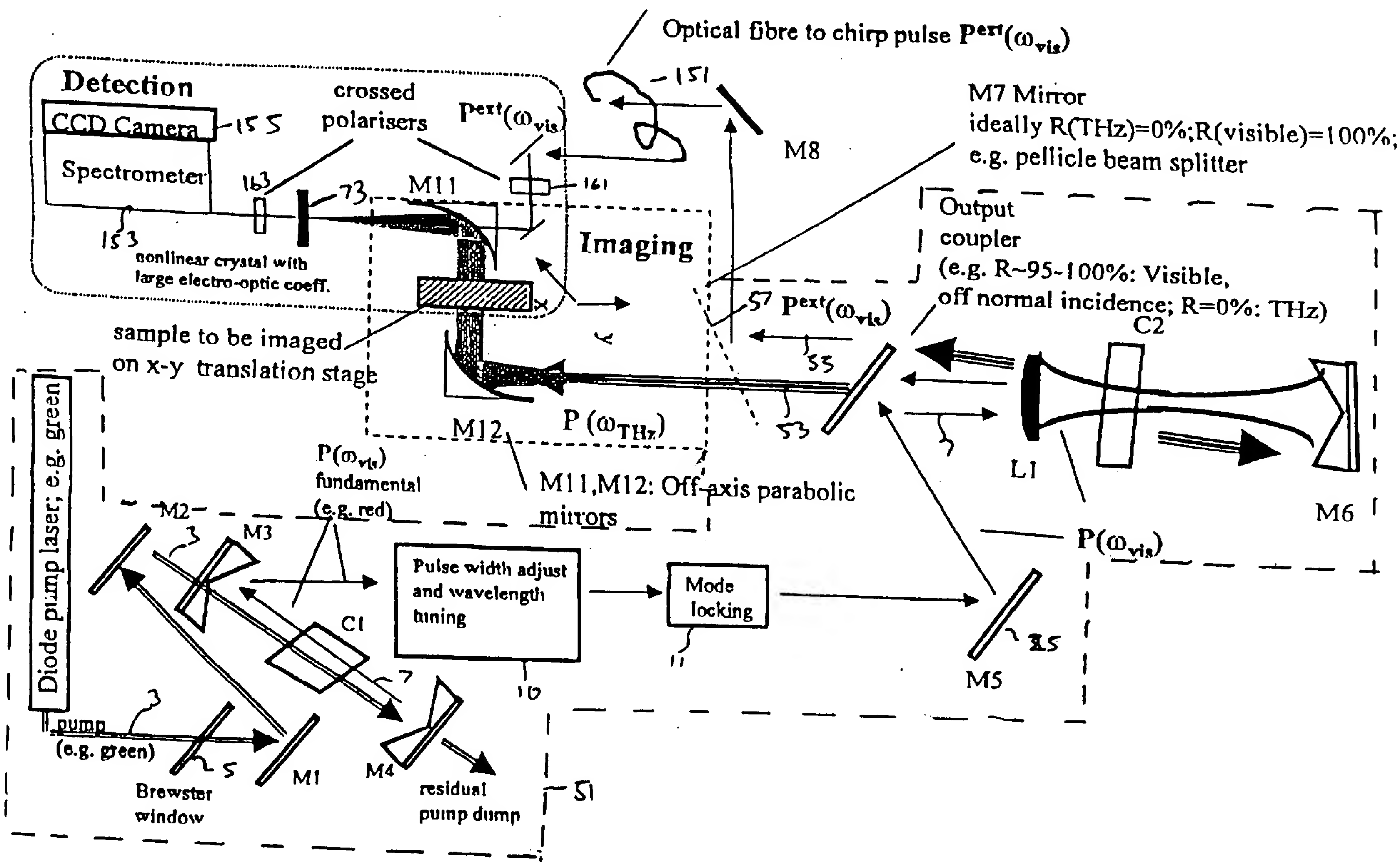

Optical fibre to chirp pulse $P^{ext}(\omega_{vis})$
151
Detection
CCD Camera
155
Spectrometer
153
crossed
polarisers
$P^{ext}(\omega_{vis})$
163
73
M11
161
nonlinear crystal with
large electro-optic coeff.
Imaging
sample to be imaged
on x-y translation stage
M8
M7 Mirror
ideally R(THz)=0%;R(visible)=100%;
e.g. pellicle beam splitter
Output
coupler
(e.g. R~95-100%: Visible,
off normal incidence; R=0%: THz)
C2
57 $P^{ext}(\omega_{vis})$
55
53
L1
M6
M12
$P(\omega_{THz})$
M11,M12: Off-axis parabolic
mirrors
$P(\omega_{vis})$
fundamental
(e.g. red)
$P(\omega_{vis})$
Diode pump laser; e.g. green
pump
(e.g. green)
M2
M3
C1
Pulse width adjust
and wavelength
tuning
10
Mode
locking
11
M5
25
Brewster
window
M1
M4
residual
pump dump
51

FIGURE 24

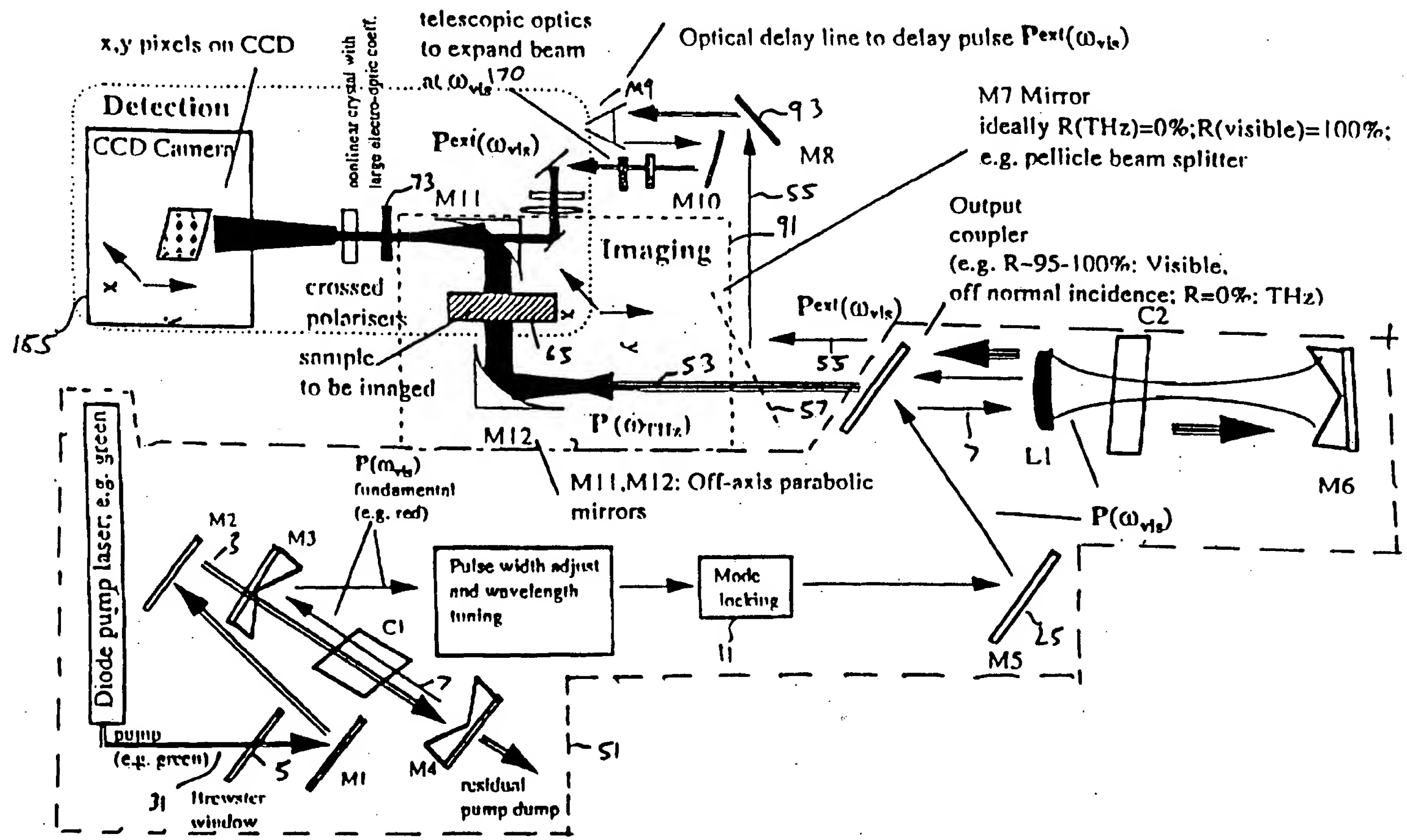

x,y pixels on CCD
Detection
CCD Camera
nonlinear crystal with large electro-optic coeff.
telescopic optics to expand beam at ω_{vis} 170
Optical delay line to delay pulse $P_{ext}(\omega_{vis})$
M9
93
M8
M10
55
91
$P_{ext}(\omega_{vis})$
73
M11
Imaging
crossed polarisers
sample to be imaged
65
53
57
155
M7 Mirror
ideally R(THz)=0%;R(visible)=100%;
e.g. pellicle beam splitter
Output coupler
(e.g. R~95-100%: Visible,
off normal incidence: R=0%: THz)
$P_{ext}(\omega_{vis})$
C2
L1
M6
7
$P(\omega_{THz})$
M12
M11,M12: Off-axis parabolic mirrors
$P(\omega_{vis})$ fundamental (e.g. red)
$P(\omega_{vis})$
Diode pump laser, e.g. green
pump (e.g. green)
31
Brewster window
5
M1
M2
3
M3
C1
7
M4
residual pump dump
Pulse width adjust and wavelength tuning
Mode locking
11
M5
25
51

FIGURE 25